TÉCNICO LISBOA

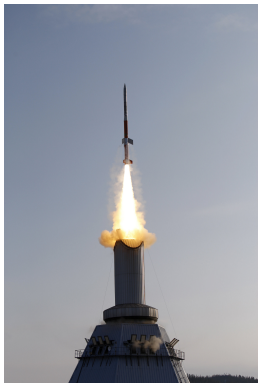

Concept design of a sounding rocket main structure using high performance materials

Pedro Miguel Gomes Silva

Thesis to obtain the Master of Science Degree in

Aerospace Engineering

Supervisors: Prof. Aurélio Lima Araújo
Dr. Eng. André Gomes da Costa Guerra

Examination Committee

Chairperson: Prof. Afzal Suleman
Supervisor: Prof. Aurélio Lima Araújo
Member of the Committee: Prof. Filipa Andreia de Matos Moleiro

December 2021

Dedicated to my family and friends who made all this possible

Acknowledgments

I would like to start by dedicating some words towards the people that helped me achieve my objective that started with my first steps in primary school and ended with the conclusion of this dissertation.

Firstly, I would like to thank all the teachers that were a part of my journey, and especially to Professor Aurélio Araújo who helped me during all the difficulties and challenges of this thesis. I would also like to thank Dr. Eng. André Guerra and Luís Pinheiro from CEiiA for their guidance during this work.

It would be impossible to conclude this journey without the help of my family, especially my grandparents, my parents and my sister who gave me all the financial and emotional support that I needed.

Finally, I wanted to thank all my friends for their help, especially the ones who lived with me during the last five years, for their help during my studies, but also all the other convivial moments.

Resumo

Nos últimos anos, tem havido um crescente interesse e investimento em tecnologias espaciais. Esse interesse tem magnitudes diferentes, desde a primeira missão tripulada a Marte, mas também uma nova era de turismo espacial. Para além disso, tem havido um aumento do investimento no lançamento de novos satélites, mas também no lançamento de foguetões para levar diferentes instrumentos de medidação ao espaço (foguete de sondagem). É neste capítulo que se insere o interesse da CEiiA, e esta tese consistiu no desenvolvimento deste foguete de sondagem. Esta tese foi desenvolvida em colaboração com o CEiiA e visa desenvolver o projeto de um foguete de sondagem, bem como o estudo de algumas componentes estruturais do mesmo. Com base nos objetivos e requerimentos da missão, e em conjunto com exemplos de outros lançadores, o projeto do foguete de sondagem foi estabelecido. De seguida, alguns componentes do foguete de sondagem foram estudados com base numa análise de elementos finitos recorrendo ao software *NX Siemens* para realizar as simulações. Este estudo foi realizado para diferentes materiais como o alumínio ou compósito reforçado por fibra de carbono e em sanduíche. Em geral, os compósitos apresentam uma solução vantajosa ao permitirem uma redução de peso mantendo a integridade estrutural do foguetão. Contudo, estes também apresentam algumas desvantagens, nomeadamente problemas de compatibilidade com o oxigénio líquido, surgindo assim o alumínio como uma solução alternativa. O trabalho desenvolvido focou-se essencialmente numa primeira iteração do foguete de sondagem e um trabalho mais detalhado é essencial para o futuro.

Palavras-chave: foguete de sondagem, compósito reforçado por fibra de carbono e em sanduíche, alumínio, análise de elementos finitos

Abstract

In recent years, there has been a growing interest and investment in new space technologies. This interest has different magnitudes, from the goals of getting the first human to Mars, but also a new era of space tourism. In addition, there has been an increasing investment in launching new satellites, but also in launching rockets to carry out all kinds of measuring instruments to space, also named sounding rocket. This is where the interest of CEiiA comes from, and this thesis consisted in the initial development of this rocket. This thesis was developed in collaboration with CEiiA and aims to develop the design of a sounding rocket, as well as the study of some of its components. Based on the mission objectives and requirements, and in conjunction with examples from other launchers, the sounding rocket design was established. Then, some of the components of the sounding rocket were studied with a finite element analysis using the *NX Siemens* software to perform the simulations based on the applied loads. This study was carried out using different materials such as aluminium and carbon fiber-reinforced polymer (CFRP). In general, composites present an advantageous solution by allowing a reduction in weight while maintaining the structural integrity of the rocket. However, composite materials also have some disadvantages, namely possible compatibility problems with liquid oxygen, thus making aluminum an alternative solution. The work developed was essentially focused on a first iteration of the rocket and more detailed work is essential for the future.

Keywords: sounding rocket, CFRP composites and sandwich, aluminium, finite elements analysis

Contents

List of Tables

List of Figures

Nomenclature

Greek symbols

ν	Poisson's ratio
σ	Stress

Roman symbols

C	Stiffness tensor
E	Young's modulus
G	Shear modulus
p	Pressure
r	Radius
t	Thickness

Acronyms

NASA National Aeronautics and Space Administration

LEO Low-Earth-Orbit

LNG Liquefied Natural Gas

LOx Liquid Oxygen

COPV Composite Overwrapped Pressure Vessel

SLS Space Launch System

TVC Thrust Vector Control

ST Allowable Tensile Stress

SC Allowable Compression Stress

SS Allowable Shear Stress

FEA Finite Element Analysis

CAD Computer-Aided Design and drafting

CAE Computer Aided Engineering

pcf pounds per cubic foot

CFRP Carbon Fiber Reinforced Polymers

ESA European Space Agency

LY Yield load

LU Ultimate load

QL Qualification load

KQ Qualification factor

LL Limit load

DL Design load

KP Project factor

KM Model factor

FOSY Yield factor of safety

FOSU Design factor of safety

Chapter 1

Introduction

In this chapter, an overview of the main topics that will be further discussed along with this thesis is provided. Besides that, a brief discussion of not only some general requirements but also some more specific objectives and deliverables is discussed.

1.1 Motivation

In recent years, there has been a beginning of a new era of space exploration like it has not been seen since the 60s and 70s which had the apogee in July of 1969 with the first arrival of a manned mission on the moon. However, this rebirth of space exploration is explained by two different reasons. The first one is similar to what happened before with the rising interest of more countries in this domain, especially countries like China, Japan, South Korea, India or the United Arabia Emirates which have joined the United States of America, Europe and Russia in the conquering of space. In addition to this, the space is now available not only to programs financed by the countries but also to private companies that are making space closer to everyone. The main companies that are leading the front of the race are SpaceX, Blue Origin, Virgin Galatic, Rocket Lab just to name a few, but there are many more gaining their share in this important area of the future like the case of CEiiA. The interest of all these private companies should be clear, especially when everyone is forecasting an increase in market value, for example, Rocket Lab [1] and Bank of America [2] are forecasting a 1.4 trillion dollar market in 2030. Communications systems, support for grounded equipment and scientific exploration are the dominant areas that will benefit from all this investment which will ultimately change the life of everyone. Rocket Lab is expecting that small satellite constellations will account for 83% of all satellites launched by 2028 [1]. For all these, the work done in this thesis in collaboration with CEiiA has a general objective of giving an extra step towards a mission where space is available to everyone. This thesis is focused on the development of a design for a sounding rocket, called ”Morpheus” (a reference to the Greek god of dreams and the popular character of the Matrix), as well as the structural analysis of some components of the rocket.

1.2 Overview of the Sounding Rocket - characteristics and requirements

1.2.1 Sounding Rocket

First of all, it is important to start by defining what a sounding rocket is. As stated by NASA [3], ”sounding rockets take their name from the nautical term ”to sound,” which means to take measurements”. A sounding rocket is a type of rocket that is especially used for a sub-orbital altitude, although sometimes they can reach altitudes of more than 1000km. However, since balloons can not reach an altitude above 40 km, and the low-Earth-orbit (LEO) satellites need to operate above 200 km to avoid re-entry due to residual atmospheric friction, sounding rockets are used to cover this range of altitudes [4].

Sounding rockets are very versatile regarding the design configuration. It is possible to have solid rocket motors, liquid rocket motor or even hybrid configurations where a solid fuel and a liquid oxidizer combination is used or vice-versa. Besides that, some sounding rockets have two or three stages. Usually the first stage of the rocket is composed of the rocket motor itself and also the fuel and propellant. The second stage is the payload where the instruments for control, recovery, the experiment and even the nose cone are present. However, sometimes a third stage is also present.

Besides the advantage of being able to reach into altitudes that are not usually accessible by neither balloons nor bigger rockets, sounding rockets are also a low-cost alternative that allows access to the microgravity environment and, due to its smaller size, this type of rocket can be launched from temporary sites in remote locations which are not possible for rockets requiring a more advanced infrastructure launching requirements.

1.2.2 Requirements

Some requirements must be followed to deliver the desired rocket capable of achieving the intended goals of CEiiA. One of the goals is to reach an altitude of 100km, and for that, the rocket will use Liquefied Natural Gas (LNG) as fuel and liquid oxygen (LOx) as the oxidizer. Since this is an unmanned mission there is no need to prepare the rocket for additional safety requirements which are necessary in case of a manned mission, besides that the margin of safety can also be smaller because the risk of life threatening accidents are much smaller. This sounding rocket will not be reusable, so there is no need for taking into account the recovery of any parts of the rocket. This rocket is going to be a single stage rocket since there is no need to deploy or separate any specific part of the rocket. Another important requirement is that the rocket should be as modular as possible, and allow a quick assemble and disassemble of the different sections to test and make any necessary changes to any of the parts. After setting the mission objectives as well as the general design features, it is important to specify some general features of this project and find the best trade-off between performance and cost. Multiple areas are important to the development of a rocket and each one of those has an impact on the others. A rocket has four major systems: payload, guidance, structural, propulsion. In this thesis the focus will

mainly be on the structural systems of the rocket, that is, to ensure that the sounding rocket will withstand the forces it will be subjected to at all times during the flight. One of the most important aspects when considering the structural aspect of the rocket and the relationship with the other areas is its mass. For this reason, the mass was one of the primary criteria in the structural analysis that will be discussed in this thesis. However, the reliability of the material, as well as, the manufacturing process are crucial to ensure that the thermal performance and the structural response are inside the window of safety that was predicted before. Regarding the cost, multiple domains can have an impact. First of all, the type of material itself can have a big impact on the price, but other areas like the cost of equipment and the manufacturing processes are also crucial.

1.3 Objectives and Deliverables

There are two main objectives of this work. The first one is to design a sounding rocket with all the requirements that were stated before. Then, the work developed under this thesis consisted of an initial study of the components of this sounding rocket, especially in the aft skirt area of the rocket.

1.4 Thesis Outline

In Chapter 1, an introduction to the topic is provided by framing the importance of this project nowadays. After that, it is explained a bit more about the role that sounding rockets have in the space industry with their advantages and disadvantages. Finally, a general introduction to the requirements and objectives of the work developed in this thesis is provided. Secondly, in Chapter 2, a literature review is discussed to provide the support work to develop the best sounding rocket possible that meets the proposed requirements. The first part of this chapter is going to be focused on the general design of previous rockets, and the second half will be discussed some more specific details regarding the choice of the materials. Then, in Chapter 3, the design of the sounding rocket will be studied in greater detail with the necessary trade-offs that were discussed. The *Solidworks* software was used to design the sounding rocket. Afterwards, the properties of some materials that will constitute some parts of the Morpheus rocket are going to be stated. Subsequently, in Chapter 4, a structural sizing of different components of the sounding rocket are studied with a special attention to the choices made to represent all the loads and details of the Morpheus' rocket design. In chapter 5, a finite element method analysis is realized to optimize each component to the best design possible with the use of the *NX Siemens*. Finally, in chapter 6, a conclusion of this thesis is stated by making an overview of the achievements and also giving a guideline to the necessary work that should be continued in the future.

Chapter 2

Literature Review - Sounding Rocket design and analysis

In this chapter, an overview of other rockets is addressed in order to support the choices in the design of Morpheus sounding rocket.

2.1 Conceptual Design - components

The design of the rocket is established starting from the nose cone to the aft skirt.

Starting with the selection of the nose cone shape, the choice depends essentially on the flight regime and how it will interact with the surrounding air and the thermal conditions that it is going to experience. As this is one of the parts of the vehicle that will have some of the hottest points of the entire vehicle especially due to the stagnation of fluid and the proximity of the Mach cones, the objective is to protect the rest of the rocket while maintaining good aerodynamic performance. However, since this thesis will be more focused on the structural system, only a brief overview of the choices in the nose cone will be provided, and more studies will be necessary for the future. Gary A. Crowell Sr. (1996) studied the different geometries of nose cones and their drag characteristics in the transonic-to-low Mach regions, which is the flight regime that the Morpheus Rocket will experience. For example, it is expected that the maximum dynamic pressure (max. Q) will occur at Mach 1.02. Even though figure 2.1 does not have information for all region velocities, it is expected that either a Power series, with $n^{1/2}$, or a Von Karman shape are good choices for the rocket. Regarding the materials in the nose cone, a structural and thermal analysis should be made, and, then choose the one with the lower mass. The nose cone is the area of the rocket that experiences the highest temperature, besides the motor, due to the aerodynamic flow during launch, so this is a critical condition in the choice of the materials used. To provide a better thermal performance a reinforcement with cork should be considered due to its low density and low thermal conductivity. Besides that, cork is also a common material in Portugal which could lower substantial the cost.

The shape of the fuselage is easier to define than the nose cone's shape. It is ideal to maintain a

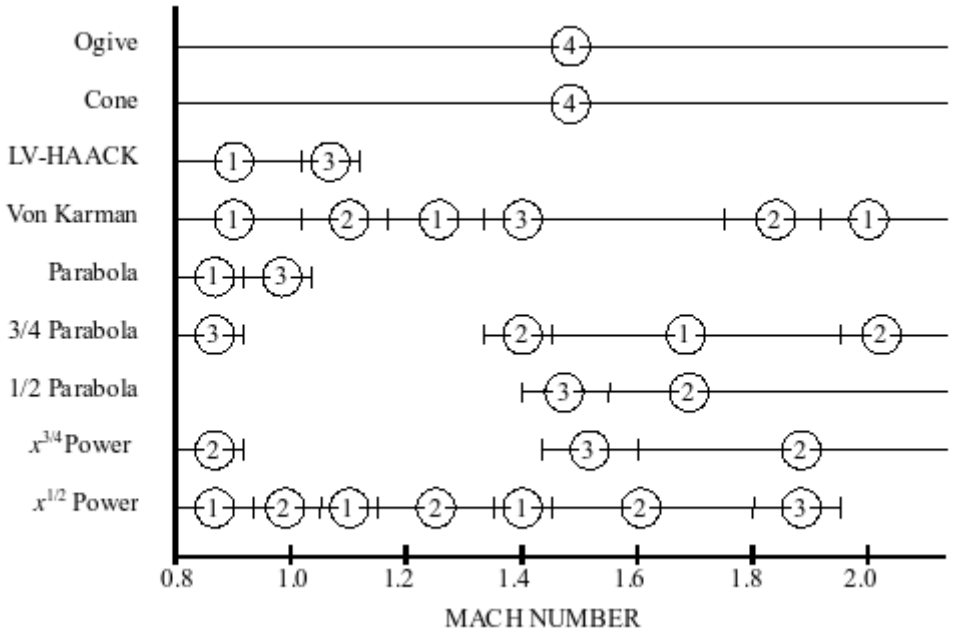

Figure 2.1: Comparison of drag characteristics of various nose cone shapes in the transonic to low-mach regions. Rankings are: superior (1), good (2), fair (3), inferior (4). [5]

circular cross-section or as close to it as possible. Cylindrical fuselage sections do not produce normal forces at zero angles of attack and, because of that, do not generate pressure drag or shock waves [6]. Besides that, the circular shape also minimizes surface area which reduces the friction drag while also keeping the pressure equally distributed which is important especially in the tanks of propellant and fuel. Finally, the circular shape is easily manufactured and offers a good load-carrying capacity. The transonic area rule establishes that transonic wave drag is minimized if the total vehicle cross sectional area remains constant over the length of the vehicle [7]. In this way, fins or any other extrusion could increase the drag resulting in the deterioration of the performance, so, to reduce the impact of an increasing cross-section due to fins or any other protrusion, a good consideration would be to decrease the diameter of the fuselage in that area.

The oxidizer and fuel tanks represent a high percentage of the total mass of the rocket when they are at full capacity and at their maximum pressure. Besides that, both tanks will contain liquids at cryogenic temperatures, the oxidizer at 90 K and the fuel at 110 K. The temperature impacts the material properties that are used and, probably, it is necessary to reinforce the tanks with a better insulation material. Besides that, the chemical compatibility must also be considered. For example, the liquid oxygen and carbon fiber reinforced composite laminates can start an ignition if not carefully managed together. This is why, aluminium is usually the material chosen for this kind of application. However, some promising results could ensure the usage of carbon fiber reinforced composite laminates in the tanks while keeping the mass lower than in an aluminium tank, since carbon fiber composites have a lower density, less than half of the aluminium [8]. In recent years, Rocket Lab has proved that is possible to produce a fully carbon fiber composite rocket, figure 2.2, so possibility for the tanks' material should be considered.

There are mainly two different ways to guarantee the insulation in cryogenic tanks. Vacuum insulation

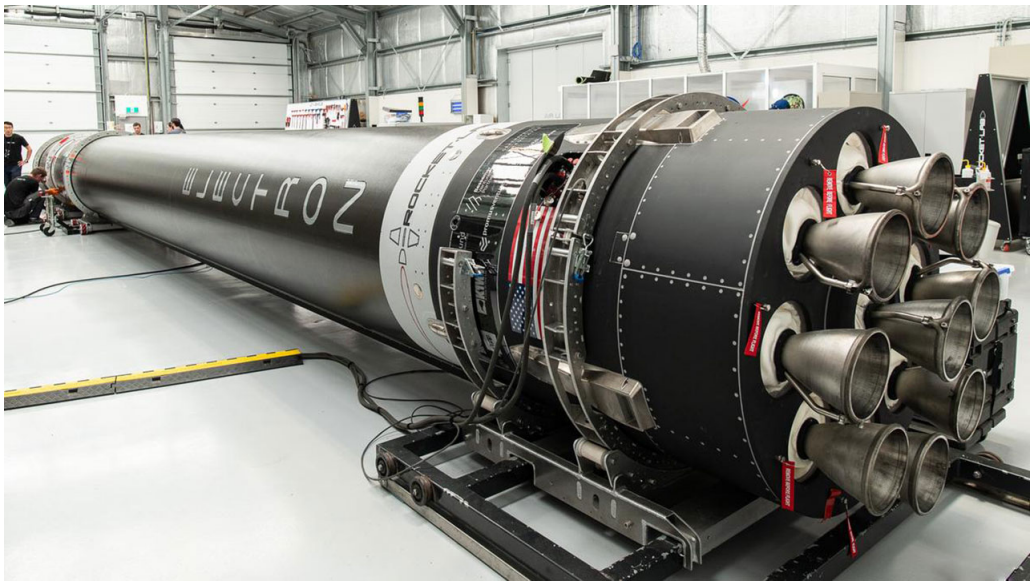

Figure 2.2: Rocket Lab Electron made of carbon-composite fiber

is one of the possibilities, this option can be reused multiple times with little damage to the structure. It has also a very good performance but is a heavy system. On the other hand, foam insulation, like poly isocyanate foam (PIF), is also a good option due to the lighter system but has an inferior performance when compared to vacuum insulation. However, the foam insulation is more susceptible to cracks. Finally, ceramic heat tiles can also be used to cover some specific parts of the rocket as those used in SpaceX Starship. Afterwards, the design of the tanks is also important. Assuming the critical failure mode is bending and not buckling, the critical (hoop) stress σ on a cylindrical shell of thickness t and radius r under internal pressure p is given by equation (2.1) [6].

$$\sigma = \frac{pr}{t} \tag{2.1}$$

Both tanks are cylindrical pressure vessels with vessel heads at both ends. These vessel heads can differ in shape depending on what is the best profile for each application. The objective when choosing the best profile possible should be to minimize mass while considering the necessary volume that will be needed and ensuring that the tank can resist the pressure. Some of the most common head types are shown in figure 2.3.

When considering the design and analysis of the rocket the temporal variation must also be considered, like fuel consumption, sloshing, stage separation and parachute deployment, however, only the first two are going to happen in Morpheus case. Besides that, the vibrations should also be minimized.

As the fuel and propellant are consumed, the pressure inside both tanks decreases. To keep the pressure constant inside the tank, a pressurization system must be used, and either an external pressurization system or autogenous pressurization can be used. The external pressurization usually uses helium contained at high pressures inside a composite overwrapped pressure vessel (COPV) to guarantee the pressurization of the tanks, figure 2.4. Helium is an inert gas and has a low density making it one of the best elements to use.

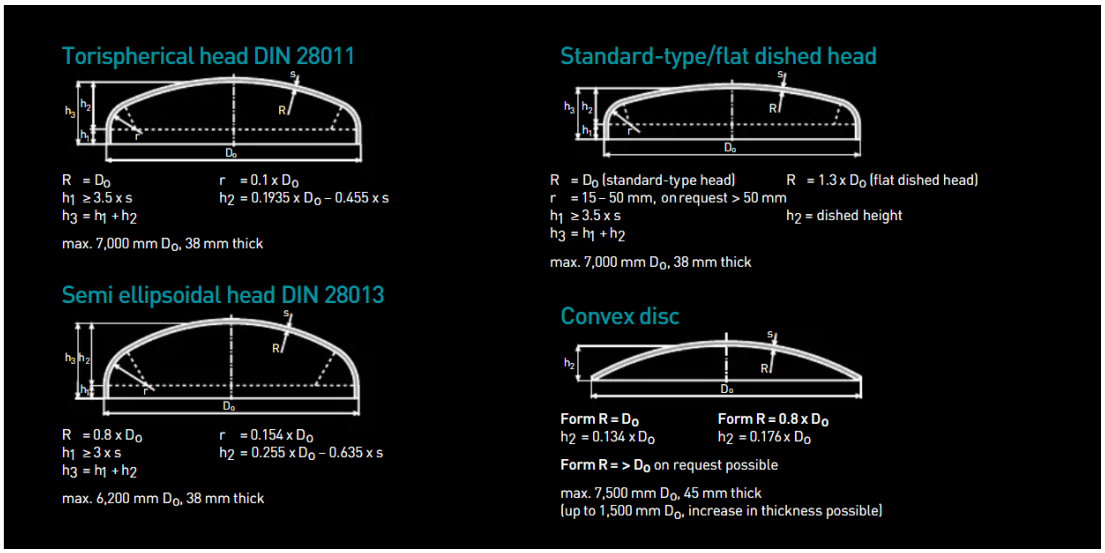

Figure 2.3: Different head types commonly used on pressure vessels

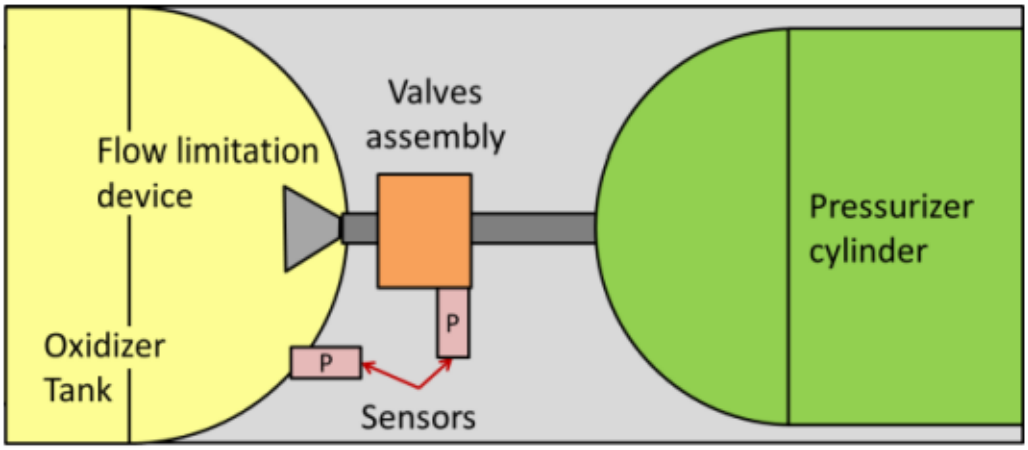

Figure 2.4: Pressurizer Feeding Section using external pressurization

On the other hand, recently the autogenous pressurization is being studied for rockets like the Space Launch System (SLS) by NASA or Starship by SpaceX, figure 2.5. This system reuses the gas from the propellant that was used in the motors to feed back into the tanks as gas to keep the pressure. This system promises some advantages since it eliminates the usage of one additional gas and is expected to lower the mass. However, some considerations should be answered, especially regarding the mass. This system eliminates the use of COPV but still needs the system to fed back the gas into the tanks, and since oxygen and the fuel are much heavier than helium, and they will be filling the tank again, this could result in a higher mass during some parts of the flight. Finally, external pressurization is a system with many years of experience making it more reliable.

To conclude, to prevent the sloshing effect caused by the movement of the liquid inside the tanks a set of slosh baffles are used inside each tank. Also, anti vortex baffles should be used inside each tank. Both of these structures are present in one of the rockets of Copenhagen Suborbitals, represented in Figure 2.6.

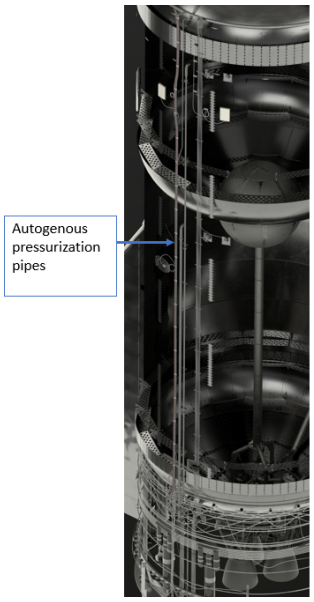

Figure 2.5: Autogenous pressurization system of early sketch of Starship

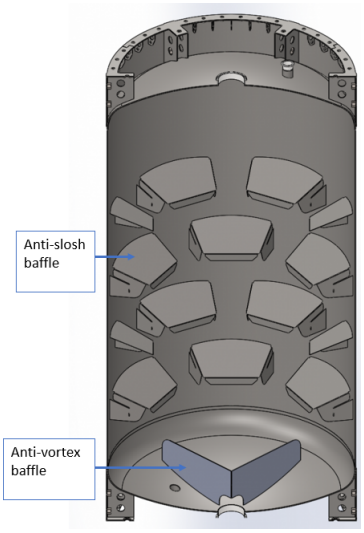

Figure 2.6: Anti-slosh and anti-vortex baffles of Copenhagen Suborbitals' rocket

2.2 Conceptual Design - complete rocket

After looking into some of the essential parts of a rocket, it is necessary to study how each of the parts will be connected. For that, two general designs are usually used in a rocket, either a skeleton design or a skin-based design. In the skeleton design, an internal skeleton gives rigidity and strength to the rocket making it the structural component. This skeleton connects all the parts of the rocket and because of that, the external skin is only an aerodynamic covering. For the skin-based design, the strength and stiffness are derived from the skin of the rocket and there is no need for an internal skeleton connecting the rocket's subsystems. In this design, the exterior skin of the tanks is also the fuselage of the rocket. This design could allow for a reduction of mass since fewer parts are used, even though a thicker fuselage should be necessary.

Another important aspect of the rocket is how the fuel will reach the motor. If the skeleton design is chosen, there could be a pipe that goes alongside the propellant tank until the motors. However, if the exterior parts of the tank are also the fuselage the pipes need to go through the outside of the rocket or pass through the inside of the LOx tank. However, the first option is more complex because it requires holes in the fuselage with pipes that go through it, making it more difficult to assemble and disassemble while also adding more unnecessary mass. So, the second option is a better option and is already being used in several rockets as is the case of the Starship of SpaceX, figure 2.7. Besides that, both LOx and LNG are at similar temperatures which removes the necessity for extra insulation.

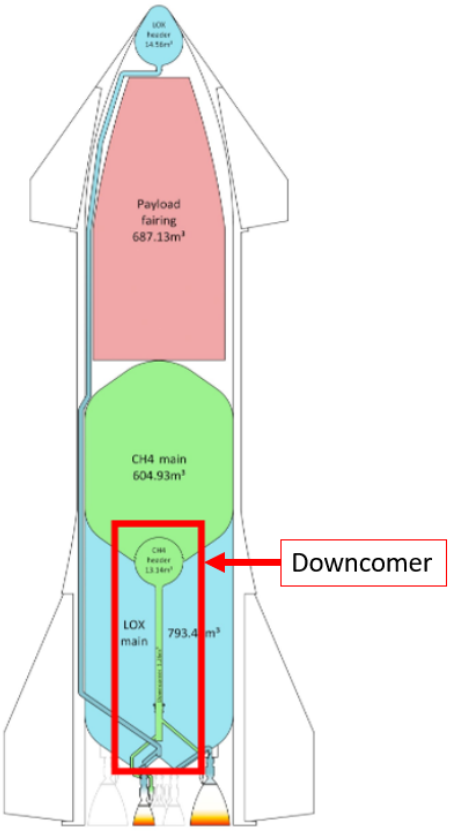

Figure 2.7: Sketch of Starship's downcomer

Now, the method to connect the different systems of the sounding rocket will be studied in more detail. There are essentially three different methods, mechanical fastening, adhesive bonding and welding.

The mechanical fastening uses mainly screws, bolts, rivets and other mechanical mechanisms. This is an easy to assemble and disassemble connection and can be applied to metal and plastic joints providing great flexibility in the design and manufacturing. However, this method increases the weight much more than the other two and promotes stress concentration in the holes.

Secondly, the adhesive bonding provides low-stress concentration, improvement of fatigue resistance and a good surface finishing while not adding much weight. Nevertheless, this process usually damages the materials themselves and when the adhesive fails, it does so instantaneously rather than in a progressive way, resulting in a lack of predictability, so, a bigger margin of safety is needed. This process is especially useful in resisting shear stress but not as good in other types of failure.

Finally, many welding techniques could be used, one of the most reliable ones for this kind of application is the friction stir welding, as stated in the Falcon 9 rocket guide, the ”highest strength and most reliable welding technique available” [9] used for welding the aluminium tanks of the Falcon 9. This welding technique does not need to reach the material melting point and does not need a filler material which is great advantage in space application since it does not add more weight. Besides that, the residual stresses and distortions developed are much lower in comparison to other welding methods. Moreover, friction stir welding offers good resistance to corrosion and does not consume the nature of the welding tool. Nevertheless, the equipment needed for this welding requires a high initial cost and needs good support tooling.

In conclusion, after analysing these three methods, although welding seems the best option to join different parts of aluminium, it may not be the best solution to connect other materials, even though recent studies have shown that is possible to use friction stir welding to join aluminium to a carbon fiber reinforced composite laminate [10]. Also, the welding does not allow for a modular design that enables a quick assemble and disassemble of different systems of the rocket. For such cases, the use of screws, rivets and bolts is considered the best option.

To join the tanks to the fuselage and to avoid making holes in the tanks and keeping the diameter of the rocket constant a ”Y-ring” like the one used in Saturn V, figure 2.8, should be studied. This aluminium Y-ring could be welded to the tanks and, then, bolted to the fuselage which could even be made out of a different material. This option allows for more flexible designs and can even be used to reinforce just some parts of the rocket.

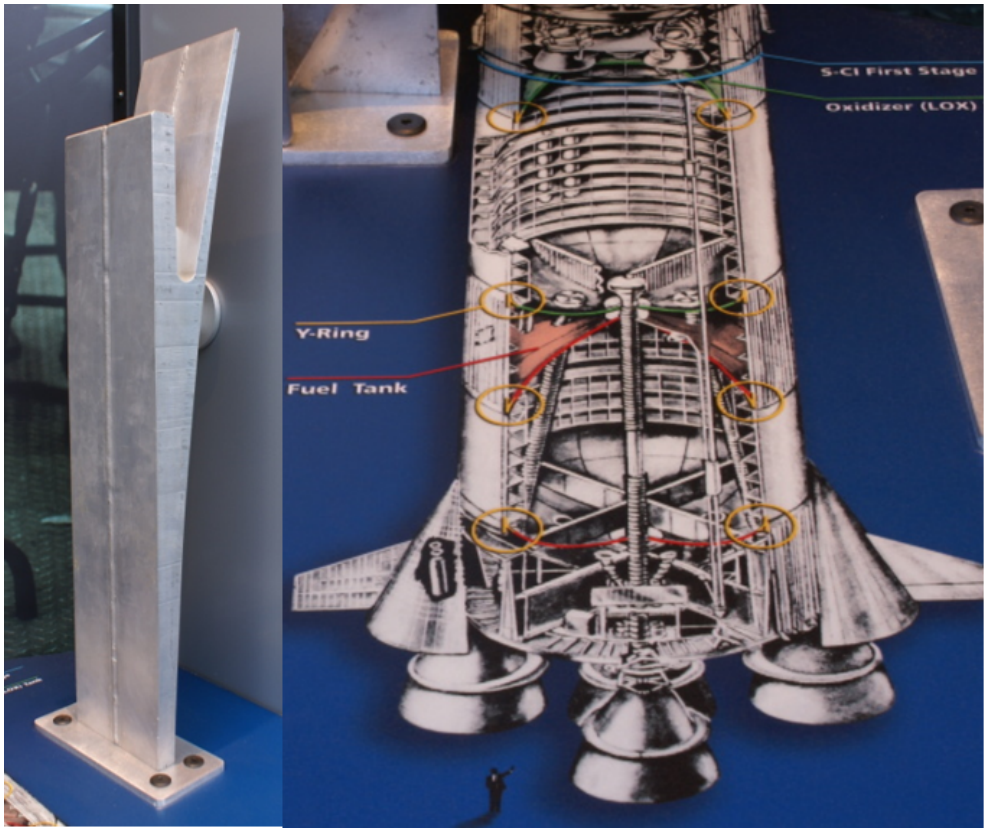

Figure 2.8: Y-ring of Saturn V

2.3 High performance materials

2.3.1 Factor of safety

Before exploring the materials in more detail, one important consideration that should be addressed to begin with is the factor of safety (FOS). This is defined by ESA as a ”coefficient by which the design loads are multiplied to account for uncertainties in the statistical distribution of loads, uncertainties in structural analysis, manufacturing process, material properties and failure criteria” [11].

The selection of appropriate factors of safety for specific components depends on the loads, design, material, manufacturing and verification parameters. Besides that, some aspects should be included when selecting the FOS such as the human presence or some special components, for example, joints, bearings and welds.

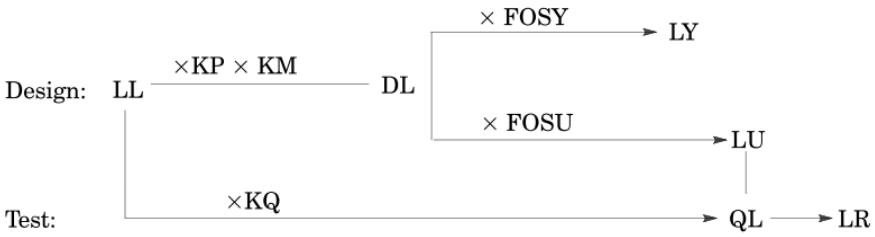

Figure 2.9: Development for a launcher structural element [11]

The definitions of some of these acronyms are the following [11]:

- LL: limit load - ”maximum load to be encountered in service with a given probability for a given design condition”
- DL: design load - ”limit load multiplied by relevant design factor”
- KP: project factor - ”accounts for possible mass increase at the start of the spacecraft design”
- KM: model factor - ”accounts for the incertitude at the start of launcher element design with respect to mathematical model used to establish the design”
- FOSY: yield factor - ”ensures an acceptable risk of yielding at limit load level during flight”
- FOSU: design factor - ”is the key factor ensuring structural reliability objective is satisfied”

Table 2.1: Factor for the development of a launcher [11]

Factor	Value
KP	1.0 - 1.3
KM	1.0 - 1.1
FOSY	1.1 - 1.25
FOSU	1.25 - 1.5

Considering all these factors, in the analysis that will be studied in this thesis, it was used the average values of KP (1.15), KM (1.05) and FOSY (1.175) which multiplied resulted in 1.42. This value could be decreased in future work, however, as this is a first study the factor of safety of 1.42 was considered acceptable

2.3.2 Corrosion, fatigue and thermal loads

Besides the structural loads that are considered in the design, other effects could cause the failure of the rocket such as corrosion, fatigue and thermal loads.

Corrosion can ”can be regarded as any deterioration in the physical and chemical properties of a material due to the chemical environment” [11]. So, it is critical to know the environment that the material will experience during the flight, but also the process of fabrication of the material themselves and the compatibility between materials that will be in contact. The corrosion could cause fretting or crack initiation which could be catastrophic.

Aluminium could be susceptible to corrosion, especially when in contact with carbon fiber reinforced composites. This happens due to galvanic corrosion. Graphite is a very noble material, while aluminium is on the opposite side of the spectrum, as shown in figure 2.10. When this occurs electric potential forms between the two materials that causes the two materials to trade electrons and ions, which results in the anode (aluminium) being corroded. This effect is even worse if the area of the cathode is very large in comparison to the anode. So, if aluminium fasteners are used in carbon fiber reinforced composite components, this could cause serious problems.

There are multiple ways to solve this problem. The most immediate answer is to look for other materials that are closer to graphite in the galvanic series. Accordingly to figure 2.10, titanium is an excellent material used in many aerospace applications due to its high specific strength, ability to withstand high temperatures and, of course, high corrosion resistance. Although titanium has a very high specific strength (ultimate tensile strength divided by density) of 77.3 [MPa/(g/cm^3)], aluminium has an even higher value of 114.8 [MPa/(g/cm^3)] [13]. As a result, if titanium is used there could be an increase in weight.

Another option would be to have an electrically insulating material between the carbon fiber reinforced polymers (CFRP) and aluminium. However, this would also add more weight. Finally, a protective coating could be applied, either by painting the surface or through an anodizing process that produces surface oxidation.

The fatigue analysis shall be performed to prevent the formation of cracks and their propagation resulting in structural failure. This problem is strongly correlated with the lifetime of each component and its reliability. However, considering that Morpheus is not a reusable rocket, the service life of each component is short, and failures due to fatigue are not expected to be predominant. Nevertheless, they shall be considered, and all the components tested and studied in an S-N curve.

The thermal loads are another critical factor that must be analysed when selecting each material to be used. A rocket experiences radical differences in temperature, not only between different sections but

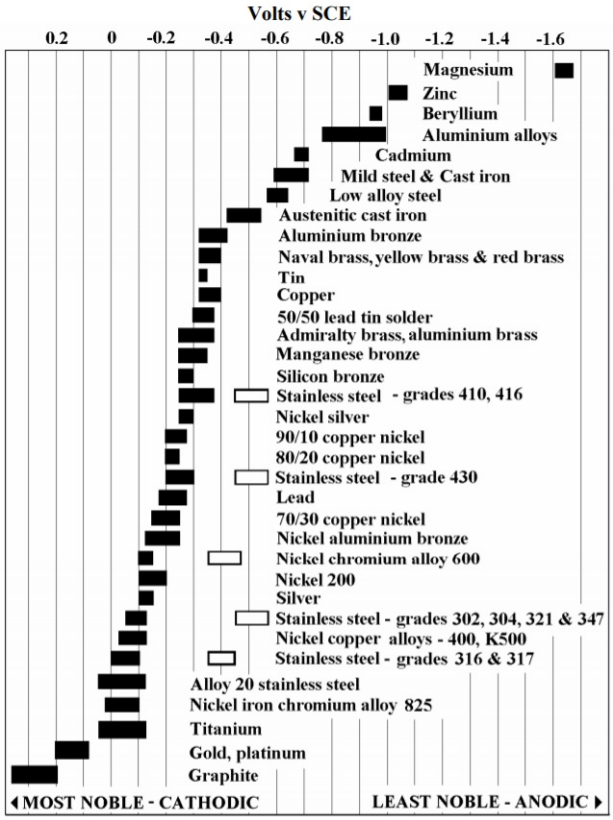

Figure 2.10: Galvanic series [12]

also through time. As an example, the tanks containing both propellant (LOx) and fuel (LNG) are kept at cryogenic temperatures, while the combustion gas is usually between 3100K and 3500K. In figure 2.11 [14], it is shown the adiabatic temperature, which is the temperature achieved by a combustion reaction without any work, heat transfer or changes in kinetic or potential energy. This temperature depends on the mixture ratio chosen, which are shown in blue, and the chamber pressure.

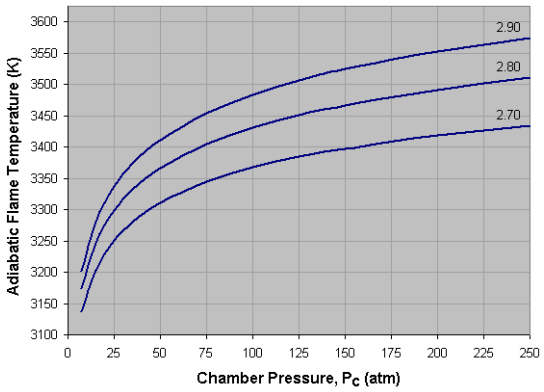

Figure 2.11: Temperature engine for LNG and LOx combination [14]

Regarding the temperatures of both the propellant and fuel tanks, which are at cryogenic temperatures of 90 K and 110 K respectively, the aluminium in general, and the Al 2219-T851 alloy, in particular, is a good choice for this purpose. The aluminium alloy increases the ultimate tensile strength for lower

temperatures. As it is shown in figure 2.12, the Young's Modulus is 76 GPa, the yield strength is 405 MPa and the ultimate tensile strength is 557 MPa for a temperature of 76 K. For reference, the main tanks are expected to be half-full tanks pressurized at 0.5MPa.

Specimen Orientation	Young's Modulus, GPa (msi)	Yield Strength, MPa (ksi)	Tensile Strength, MPa (ksi)	Elongation %	Reduction of Area %	Fracture Toughness MPa/m (ksi/in)
			295 K			
T	75 (10.9)	331 (48)	443 (64)	8	16	
L	72 (10.4)	342 (50)	447 (65)	8	19	
S	—	—	469 (68)	—	11	
						ASTM E 813
T-L						30 (27)
L-T						31 (28)
						ASTM E 1304
T-L						38,38,38 (35,35,35)
L-T						49,48,48 (45,44,44)
S-L						29,29,26 (26,26,24)
S-T						31,27,33 (28,25,30)
			76 K			
T	76 (11.0)	405 (59)	557 (81)	9	16	
L	78 (11.3)	409 (59)	556 (81)	10	22	
S	—	—	570 (83)	—	9	
						ASTM E 813
T-L						38 (35)
L-T						41 (37)
						ASTM E 1304
S-L						32,28,28(29,25,25)
S-T						34,30,31(31,27,28)
			20 K			
T	87 (12.7)	424 (61)	649 (94)	11	17	
L	82 (11.9)	430 (62)	642 (93)	11	17	
			4K			
T	82 (11.9)	434 (63)	660 (96)	9	15	
L	81 (11.7)	439 (64)	662 (96)	10	18	
S	—	—	629 (91)	—	—	
						ASTM E 813
T-L						36 (33)
L-T						42 (38)
						ASTM E 1304
T-L						44,43 (40,39)
L-T						58,54 (53,49)
S-L						31,30 (28,27)
S-T						33,32 (30,29)

Figure 2.12: Tensile and toughness properties: Al 2219-T851[15]

The CFRP also have good mechanical properties at cryogenic temperatures. As it is shown in figure 2.13, when considering the quasi-isotropy category and a cryogenic temperature of 77 K, this material has a Young's Modulus of 51.92 ± 3.0 GPa, and an ultimate strength of 620.83 ± 51.60 MPa [16]. These values are not very distant from those of aluminium alloy, and considering the possibility of a big weight saving with CFRP, this is a possibility that should be taken into account. In some studies, it was shown that composite cryogenic tanks can achieve weight reductions up to 40 % compared with metal tanks [17, 18].

However, the greater problems with CFRP cryogenic tanks are not the mechanical properties themselves, but rather the incompatibility, especially with liquid oxygen, low-temperature cracking and the leakage problems, in the process of manufacturing composite cryogenic tanks.

The incompatibility with liquid oxygen derives from two reasons. Firstly, the composites may suffer from brittle failures and cracks under cryogenic temperatures. Then, the strong oxidation of liquid oxygen can cause combustion, sparks and explosions when subjected to external effects, such as collisions, friction and static electricity [19]. One of the solutions to this problem is to use a modified epoxy resin matrix that is flame retardant. The main elements that are being added to the pure epoxy resins are bromine, phosphorus, silicon, nitrogen and the combination of phosphorus and silicon [19]. All of

Category	Temp.	Moduli-Exp GPa	Moduli-FEA GPa	Error %	US-Exp MPa	US-FEA MPa	Error %
Unidirectional-0	RT	150.83 ± 2.62	160.61	6.48	2181.31 ± 29.29	2200.59	0.88
	173 K	138.48 ± 5.02	153.38	10.76	1867.34 ± 45.92	2026.40	8.52
	77 K	139.72 ± 10.28	147.33	5.45	1828.42 ± 102.46	1759.08	3.79
Unidirectional-90	RT	8.76 ± 0.12	8.92	1.83	56.55 ± 4.02	57.34	1.40
	173 K	11.34 ± 0.79	12.31	8.55	55.63 ± 2.31	56.92	2.32
	77 K	15.39 ± 1.10	14.93	2.99	53.15 ± 6.73	56.86	6.98
Quasi-isotropy	RT	55.54 ± 1.77	56.66	2.02	829.75 ± 6.52	791.88	4.56
	173 K	54.84 ± 3.09	55.40	1.02	710.24 ± 48.33	723.74	1.90
	77 K	51.92 ± 3.00	54.89	5.72	620.83 ± 51.60	657.59	5.92

* US: Ultimate Strengths; Temp: Environment temperatures.

Figure 2.13: CFRP mechanical properties [16]

these elements have advantages and disadvantages, and many investigations are currently ongoing to improve this solution.

Secondly, composites are susceptible to microcracks under low-temperature conditions. These microcracks are very problematic because they can allow leakages of the fluids inside the tanks or even expand and lead to the destruction of the overall component. These microcracks derive from the concentration of stress between plies or between the carbon fiber and the epoxy resin. The thermal cycles of low and high temperatures increase the probability of the appearance of these cracks. Similarly to the incompatibility problem, in this case, one of the solutions is also to modify the epoxy resin. Some of the most common methods are rubber elastomer toughening, thermoplastic resin toughening, core–shell particle toughening, hyper-branched polymer toughening, flexible segment toughening and nano-material toughening [19].

Besides that, the liquid fuel and propellant can leak from the tanks essentially due to two main reasons, either through diffusion leakage, in which liquid molecules diffuse through the free volume in composites, or microcrack leakage. To solve these problems, there should be paid close attention to the toughness of interlayers and the optimization of the laminate structure, for example by analysing the ply angle and thickness of each laminate [19].

There is still a lot of research that should be done in this area, especially in the study of the fibers and resin matrixes and their properties, but also in the manufacturing process of these components for aerospace applications. Although these options show promising results, the composite solution is not as reliable as the aluminium options which has decades of use and experience in aerospace applications.

In contrast, when the temperature increases, the mechanical properties of both aluminium 2219-T851 and CFRP become weaker. The aluminium alloy has an ultimate tensile strength of 455 MPa at room temperature (24° C), 338 MPa at 149° C and only 30 MPa at 371° C [20]. Jie Xu et al. [21] tested a high-temperature-resistant (HTR) CFRP and also showed a decrease in both the tensile strength and tensile modulus, figure 2.14. However, this result can be explained by the softening of the matrix.

These results show that for both materials, in areas where high temperatures are expected, such as the nose cone or the motor, it is necessary additional thermal insulation.

Temperature (℃)	Strength (MPa)			Average strength (MPa)	Retention ratio
	S-1	S-2	S-3		
20	2680.42	2696.21	2648.33	2674.99	1.00
80	2587.85	2600.59	2563.06	2583.83	0.97
150	2441.43	2218.61	2546.47	2402.17	0.90
200	2040.36	2123.12	2059.46	2074.31	0.78
250	1575.63	1534.25	1464.22	1524.70	0.57
300	1088.62	1158.65	1069.52	1105.59	0.41
350	954.93	1056.79	945.35	985.69	0.37
400	1024.96	964.45	1028.11	1005.84	0.38
450	980.39	891.27	932.65	934.77	0.35
500	751.21	633.41	687.55	690.72	0.26
600	458.37	471.10	592.06	507.17	0.19

(a)

Temperature (℃)	Modulus (GPa)			Average modulus (GPa)	Retention ratio
	M-1	M-2	M-3		
20	170.48	180.11	178.32	176.30	1.00
80	164.27	159.14	161.38	161.60	0.92
150	165.30	174.92	166.94	169.05	0.96
200	159.31	159.55	169.01	162.62	0.92
250	128.69	167.15	150.82	148.89	0.84
300	136.18	152.83	146.44	145.15	0.82
350	81.01	87.42	–	84.22	0.48

(b)

Figure 2.14: (a) Tensile strength of HTR CFRP (b) Tensile modulus of HTR CFRP

2.3.3 Sandwich structure

The most basic sandwich structure can be defined as follows: ”a sandwich is a three-layered structure consisting of an upper and lower face skin and an intermediate sandwich core”, figure 2.15 [22]. The skin and the core, which in this thesis is a hexagonal honeycomb, are bonded by adhesive sheets.

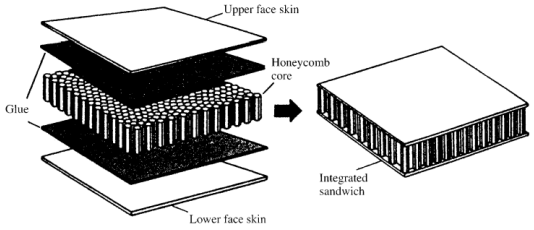

Figure 2.15: Sandwich structure [22]

The face skins are characterized by their strong resistance in tension and compression, while the core main role is to ensure a high bending stiffness with a low-density material. However, with the increase in the core thickness, it is also expected a contribution to the overall in-plane stiffness. But the effective core stiffness is a nonlinear function of the total core thickness as a result of the core deformation and displacements relative to the skin. The effect of the core thickness is shown in figure 2.16. As the thickness of the honeycomb core increases, the in-plane properties become more isotropic with a significant reduction of the C_{yy}, due to ”the strong displacement coupling of the core with the face skins and thus the marked discrepancy between the core displacements directly at the face skins and those far away from the face skins”. On the other hand, the C_{xy} registers an increase while the C_{xx} has a small reduction with the increase in thickness.

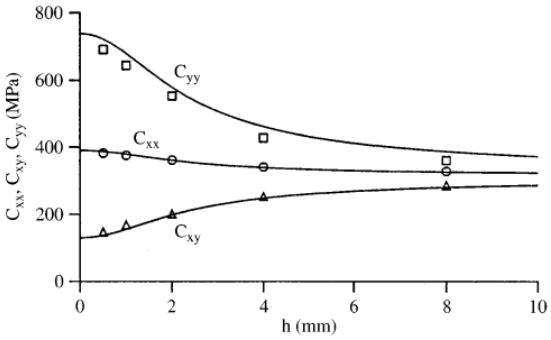

Figure 2.16: Effect of the core thickness h in the core stiffness C_{xx}, C_{yy}, C_{xy}

In the analysis that will be done during this thesis, the properties of the honeycomb were kept constant regardless of the thickness of the honeycomb. This does not correspond entirely to the real case as it is demonstrated in this section, so a careful approach should be taken when increasing the thickness of the honeycomb. Besides that, an increase in thickness also increases the manufacturing difficulty and the probability of debonding.

Chapter 3

Morpheus design

The following sections of this chapter will describe the initial design of the Morpheus rocket. Besides that, it will also be described in more detail the properties of some materials. The *Solidworks* software was used to design the components of Morpheus.

3.1 Conceptual Design

In this section, it will be explained the process and the choices that were made until the final design of the sounding rocket was achieved. This is an iterative process and there are some points that still require a deeper analysis to pursue the best possible rocket. Also, it is important to note that this is a general design and does not include all the details, but only a first design of each section of the rocket and how they will be joined together. Some areas are not represented such as the avionics or the cables and tubes that must be present for a more detailed design, especially in the motor. The motor was not studied during the work presented in this thesis and, only a representation of the motor is shown. In this first step, the objective was to get a general idea of the full rocket design and only after that start to iterate in more particular areas. The first design of the rocket is not expected to be the final one due to the iterative process, and because of that, in this section, the benefits and drawbacks of each choice will be analysed.

The main sections of the rocket, the nose cone and both the propellant and fuel tanks are the starting point of the design of the rocket. In chapter 2, it was presented the advantages and disadvantages of an aluminium or a CFRP tank. Aluminium has been used for many decades in the aerospace industry making it a reliable option, besides that it is easy and cheap to manufacture. On the other hand, a CFRP would allow for a weight reduction but would need further study on the impact of cryogenic temperatures as well as possible compatibility issues with the fuel and propellant. To reduce the cost, save time and guarantee a safer option it was chosen that the tanks should be made out of aluminium. Besides that, the nose cone could be made out of CFRP composite laminates with some thermal protection to obtain the lightest model possible while delivering the aerodynamic performance desired. After defining these three sections, the next step was to define the sections that would separate the nose cone from the

propellant tank which also corresponds to the location of the avionics, then the inter-tank section and, finally, the aft skirt where the motor is going to be located. These last three different sections do not need to withstand very high or very low temperature, neither big pressures, so they can be very light since they only need to resist the weight of the rocket and the elevated acceleration of the rocket itself. For these reasons a CFRP composite laminate should cover the skins with a possible reinforcement in some specific areas. However, since the tanks are made out of aluminium and these sections are made of CFRP composite laminates, the connection them should be with screws while also allowing for a quick assemble and disassemble.

It is extremely important to ensure that the desired pressure inside both tanks is maintained to guarantee that the propellant and fuel are kept in a liquid state. Also, the tanks are maintained at this high pressure in consequence of the high amount of both liquid natural gas and liquid oxygen that are kept inside the low volume tanks. Because of that, any hole should be avoided in the tanks to prevent any leakages and to maintain the low temperature as required. Due to these conditions, a Y-ring part of aluminium, figure 3.1, must be welded to the tank which will then be used to connect the fuselage in the avionics section with the propellant tank. In figure 3.1, it is also shown the connection between the y-ring and the fuselage, through a female rivet nut and a screw. Also, the nose cone and the fuselage of the avionics will be joined together through screws to avoid the difficult welding process in CFRP while allowing for a quick assemble and disassemble of the rocket, figure 3.2. In the figures below, the colour blue was used to better distinguish between the different components, besides that it was also used some transparency and section views to see the inside of the rocket.

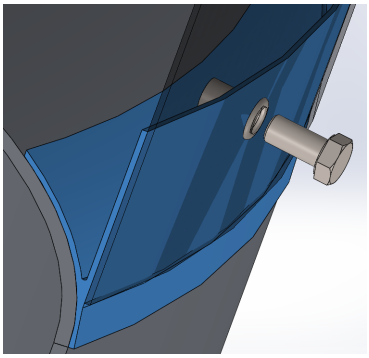

Figure 3.1: Y-ring (in blue), rivet and bolt

Inside the fuselage of the avionics section, a support of CFRP will be used to mount all the avionics needed, for that a component with an ”L-shape” will be screwed to the fuselage and to this support, figure 3.3. Furthermore, a small door will allow for a quick access to the avionics as well as to the top of the propellant tank, figure 3.4. Through that door, the propellant tank will be filled before launch. The support for the avionics should not need to withstand high stresses, so this component was designed with some holes to reduce some weight, as shown in figure 3.5.

In the section between the propellant and the fuel tank, the same approach as before was designed, with an aluminium Y-ring welded to the bottom of the propellant tank, and another one to the top of the fuel tank. After that, a CFRP fuselage should be connected to both tanks through screws that go across

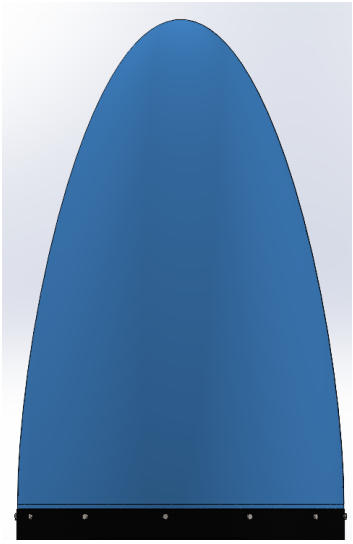

Figure 3.2: Nose cone (in blue)

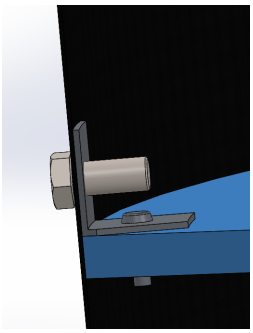

Figure 3.3: L-shape component

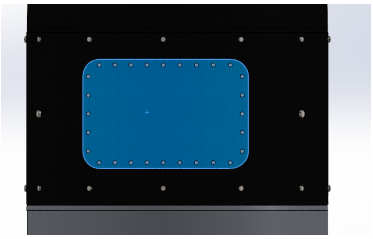

Figure 3.4: Door (in blue)

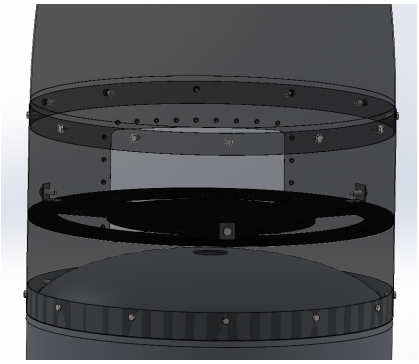

Figure 3.5: Avionics section with the support for the avionics

the y-ring, figure 3.6. In this section, the tube that came from the propellant tank must be connected with screws and nuts to the downcomer that will go through the fuel tank to deliver the liquid oxygen to the motor, figure 3.7. Moreover, a small door would also be present in this section for the same reasons as stated before, the possibility of quick access to this section of the rocket and a passage for the tube to fill the fuel to the tank.

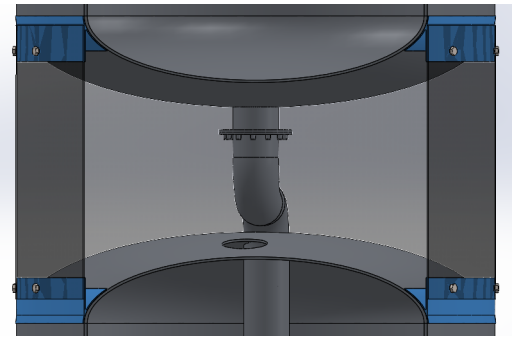

Figure 3.6: Inter-tank section

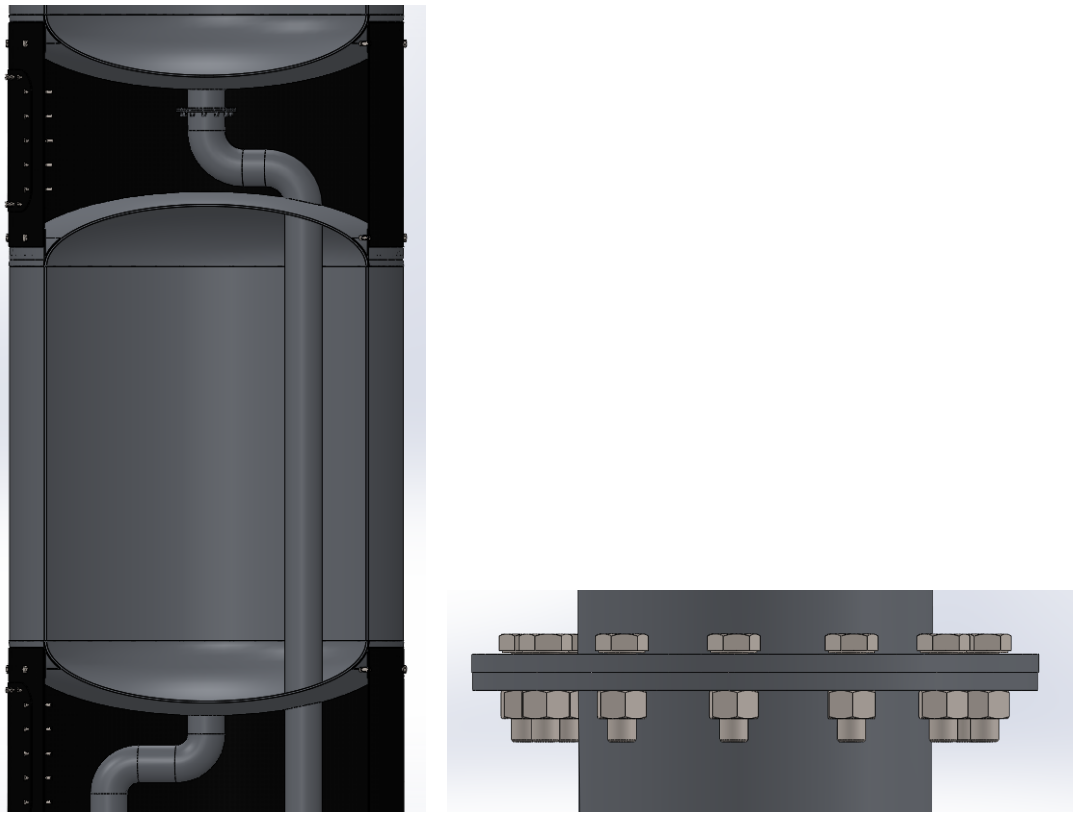

(a) (b)

Figure 3.7: (a) Downcomer going through the fuel tank (b) Detailed connection of the downcomer

Finally, the bottom part of the fuel tank will be welded to a Y-ring that should then be screwed to a fuselage skin. A support is going to be mounted into the fuselage skin to support the motor of the rocket, figure 3.8. A more detailed analysis will be described in sections 4 and 5 to reach at the best design for either the support of the motor and the fuselage skin of the aft skirt. In this section, a door

is going to allow a quick access to the motor as in the sections mentioned before. The final design of the sounding rocket is shown in appendix A, figure A.1 and A.2. The nose cone, the different doors, the fuselage (except the tanks) and the supports for the avionics and motor are initially designed to be made out of CFRP composite laminates with the possibility for some reinforcements in specific areas. As it was mentioned in section 2, the exterior of the tanks would also be considered as the fuselage. The tanks should also have anti-vortex and anti-slosh components but these parts were not represented in the final design.

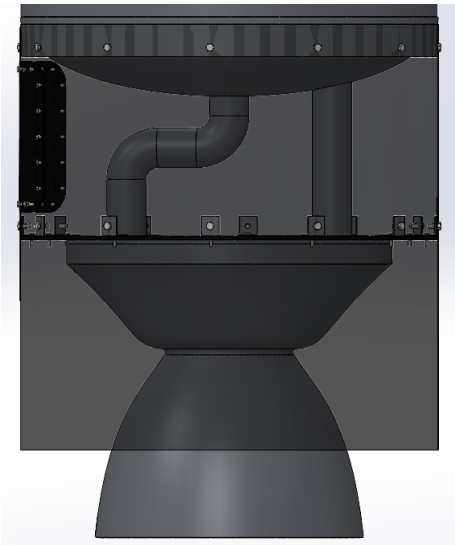

Figure 3.8: Aft skirt region with the motor

In this design, it is not represented any composite overwrapped pressure vessel (COPV), but they should be placed at the top of each tank to keep the pressure constant inside the tanks. Besides that, the electronic cables that go through the sounding rocket should go over the exterior of the rocket through small holes in the fuselage. These small holes should not cause any structural problems since they are not located in critical areas like the tanks. However, a more detailed study should be done in future work.

Another important characteristic that should be taken into consideration when joining different components is the thickness and accessibility of those same components. Since the thickness is too small to have a screw thread, a female rivet nut is first applied and then the screw or rivet male is screwed to the female rivet, joining the two components in this way (shown in figure 3.1). This is also helpful because it does not require access to the interior of the rocket to apply neither the rivet nor the screw. This method was planned to join every component of the rocket except for the downcomer, where a screw and a nut are applied to guarantee that there are no leaks of fluid in the downcomer connection (shown in figure 3.7(b)) and also in the welding between the y-ring and the aluminium tanks.

3.2 Material

Due to the requirements and the design constraints, three different materials were selected to study the lightest configuration possible while assuring that the vehicle would withstand the forces during all

phases of the flight of Morpheus. These materials are aluminium, more specifically an aluminium 2219-T851, CFRP unidirectional lamina and a HexWeb® Aluminum Flex-Core® honeycomb [20] which uses either 5052 or 5056 alloy foil material with two cell sizes. The aluminium 2219-T851 is an isotropic material and its properties were previously provided by CEiiA, as shown in Table 3.1. Besides that, it is also necessary to define the ultimate tensile strength of aluminum. Based on the MatWeb data sheet, an aluminum plate with a thickness between 6.35 mm and 50.8 mm has an ultimate tensile strength of 425 MPa [23]. On the other hand, to model the tanks, it was taken into consideration the temperature which is considered to be 90 K for the LOx tank and 110 K for the LNG Tank. The ultimate tensile strength for these temperatures was calculated with a linear interpolation based on the values of table 3.2 of MatWeb data sheet [23].

Table 3.1: Aluminium 2219-T851 properties

Modulus of elasticity [GPa]	**Shear modulus [GPa]**	**Poisson's ratio**	**Density [kg.m^{-3}]**	**Thermal expansion coefficient [K^{-1}]**	**Reference temperature for thermal loading [K]**
73.1	27.0	0.33	2840	2.41E-05	300

Table 3.2: Ultimate tensile strength for different temperatures of aluminium, based on MatWeb datasheet

	Temperature [$^\circ$ C]	**Ultimate Tensile Strength [MPa]**
Provided	-80.0	490
Calculated	-163.15	548.8
Calculated	-183.15	562.9
Provided	-196	572

The properties of the CFRP unidirectional lamina were also previously provided by CEiiA and some considerations need to be taken into account to analyse some components in *NX Siemens* software. For the first analysis of Morpheus' components, it is a good approximation to consider a CFRP lamina as an orthotropic material. The mechanical properties are available in Table 3.3, such as the Young's Modulus (E), shear modulus (G) and Poisson's ratio (ν, in *NX Siemens* is referred to by the GU symbol). However, the Poisson ratio was considered the same in all directions since it was only given one value and it is a good approximation for this kind of analysis. The allowable tensile stress (ST), compression stress (SC) and shear stress (SS) are shown in Table 3.4. The CFRP lamina density is 1210 kg.m^{-3} and the failure criteria used was the Tsai-Wu.

From all the available types of HexWeb® Aluminum Flex-Core® honeycomb that are shown in figure 3.9, it was chosen the 5056 aluminium alloy with a material/cell count -gauge of F80-0.0023 with a density of 8 pcf. Although the first criteria to choose the type of aluminium honeycomb was the lowest density, it was only possible to choose one of the densest honeycombs (128.15 kg/m^3) due to the mechanical properties, since the other types of honeycomb required a much bigger thickness of the honeycomb. If the thickness of the honeycomb is too large, around 25 mm or more, more problems

Table 3.3: CFRP unidirectional lamina: mechanical properties

E_1 [GPa]	**E_2 [GPa]**	**E_3 [GPa]**	**G_{12} [GPa]**	**G_{13} [GPa]**	**G_{23} [GPa]**	ν_{12}	ν_{13}	ν_{23}
66.8	70.0	70.0	5.50	2.70	2.70	0.071	0.071	0.071

Table 3.4: CFRP unidirectional lamina: Stress limits

ST_1 [MPa]	ST_2 [MPa]	ST_3 [MPa]	SC_1 [MPa]	SC_2 [MPa]	SC_3 [MPa]	SS_{12} [MPa]	SS_{13} [MPa]	SS_{23} [MPa]
264	241	241	295	280	280	38.3	20	20

	Material/ Cell Count – Gauge	Nominal Density pcf	Compressive Strength					Crush Strength psi	Beam Shear Strength					
			Bare		Stabilized				L Direction			W Direction		
			Strength psi		Strength psi		Modulus ksi		Strength psi		Modulus ksi	Strength psi		Modulus ksi
		typ	typ	min	typ	min	typ	typ	typ	min	typ	typ	min	typ
	F40 – .0013	2.1	200	126	225	157	65	80	90	63	18.0	50	37	10.0
	F40 – .0019	3.1	360	238	395	280	125	165	170	126	32.0	100	75	13.0
5	F40 – .0025	4.1	525	378	560	420	185	250	260	182	43.0	150	115	17.0
0	F40 – .0037	5.7	935	630	1050	700	290	380	400	280	68.0	230	170	23.0
5	F80 – .0013	4.3	524	402	542	455	195	–	300	196	45.0	190	120	20.0
2	F80 – .0019	6.5	1200	700	1300	735	310	–	540	308	72.0	310	180	24.0
	F80 – .0025	8.0	1600	1100	1750	1120	400	–	650	434	98.0	455	260	31.0
	F80 – .0037	12.0	2700	2300	2600	2200	–	1500	1450*	1100*	160	1200*	825*	71.0
	F40 – .0014	2.1	240	150	260	182	65	–	105	74	18.0	55	42	10.0
5	F40 – .0020	3.1	460	284	465	329	125	–	200	150	32.0	120	90	13.0
0	F40 – .0025	4.1	680	440	740	483	185	–	310	217	45.0	200	132	17.0
5	F80 – .0014	4.3	780	475	860	518	195	–	375	235	47.0	240	138	20.0
6	F80 – .0020	6.5	1400	805	1500	910	310	–	645	364	73.0	420	213	24.0
	F80 – .0023	8.0	1800	1210	1950	1260	410	–	850	518	100.0	570	307	32.0

*Note - * Results using Beam Shear*

Figure 3.9: HexWeb® aluminum flex-core mechanical properties (typical values (typ) as well as minimum average (min)

need to be considered. Furthermore, the standard thickness of the honeycomb for this supplier [20] ranges from 6.35 mm to 101.6 mm, however it is possible to get other dimensions for the honeycomb on request. From the available data, as needed for the analysis described in Chapter 4, it was used the values of the minimum average that are shown in figure 3.9, for a more conservative approach. Since some of the properties were not given in the available datasheet such as the Young's modulus in direction 1 and 2 and inplane shear modulus, and because they are required to perform the calculations in the *NX Siemens* software, it was considered a small value (0.01 MPa) for these parameters, which is a good approximation considering that the main objective of the honeycomb is to resist shear loads and buckling and it is very weak in those directions (1 and 2) when compared to the modulus in the vertical direction, direction 3. Since the Poisson's ratio in the directions 13 and 12 is not required for the calculations, it was not introduced in the software. As for the stress limits, the available values were introduced to the software and for the others it was considered a negligible value of 0.01 MPa which is a good approximation for this honeycomb, as shown in Table 3.5 and Table 3.6.

One of the advantages of this Flex-Core® honeycomb is that it permits a "small radii of curvature without deformation of the cell walls or loss of mechanical properties" [20], as is shown in figure 3.10.

Hexcel also offers a "vented "Flex-core. The vented structures offer thermal protection due to the low thermal conductivity while also preventing the pressure from debonding the sandwich structure, as it is shown in figure 3.11. "The venting is a rectangular shaped vent in the free cell wall of the flexcore honeycomb" [20].

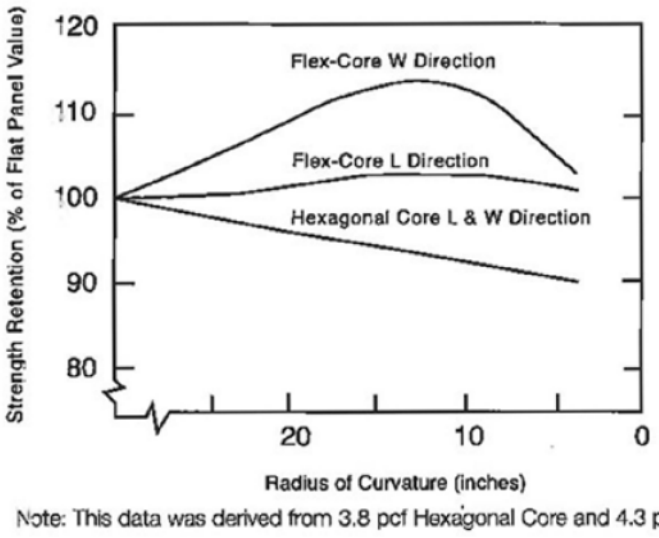

Figure 3.10: Effect of the radius of curvature in the strength retention [20]

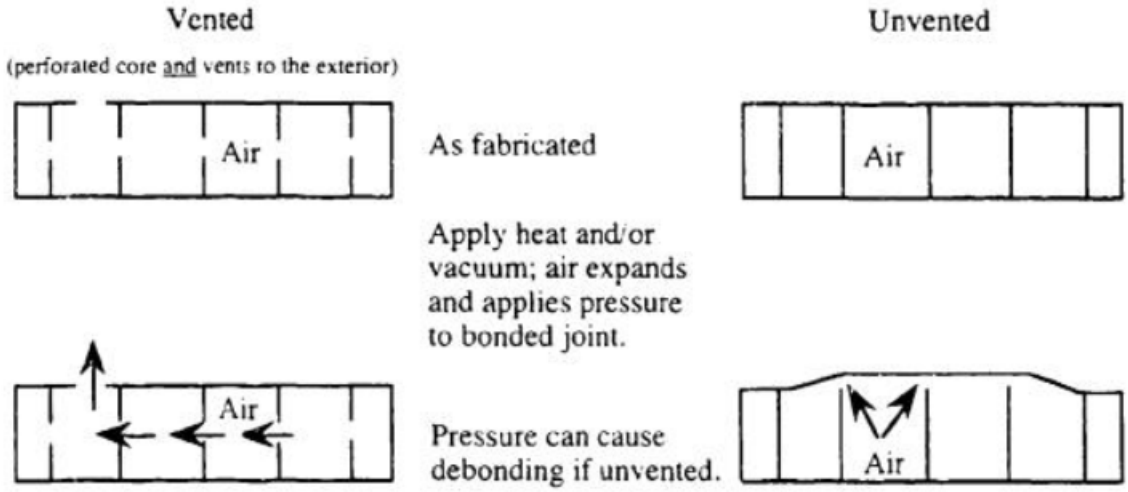

Figure 3.11: Vented versus unvented honeycomb structures

Table 3.5: HexWeb® Aluminum Flex-Core® honeycomb: mechanical properties

E_1 [MPa]	E_2 [MPa]	E_3 [MPa]	G_{12} [MPa]	G_{13} [MPa]	G_{23} [MPa]	ν_{12} [MPa]	ν_{13} [MPa]	ν_{23} [MPa]
0.01	0.01	2826.85	0.01	689.48	220.63	0.49	—	—

Table 3.6: HexWeb® Aluminum Flex-Core® honeycomb: Stress limits

ST_1 [MPa]	ST_2 [MPa]	ST_3 [MPa]	SC_1 [MPa]	SC_2 [MPa]	SC_3 [MPa]	SS_{12} [MPa]	SS_{13} [MPa]	SS_{23} [MPa]
0.01	0.01	0.01	0.01	0.01	8.34	0.01	3.57	2.12

Chapter 4

Structural Sizing

This chapter will start by describing the operational loads that will be present during the launch of the vehicle and which ones of those are going to be analysed in the simulations that will be followed. Besides that, an initial description of the finite element analysis will be presented with a more detailed overview of each component (thrust frame and aft skirt), especially the different meshes and connection elements used.

4.1 Operational Loads

A case study with all the operational loads was provided by CEiiA, and all the detailed information is in Table A.3 of the appendix. The information that is shown in a green cell represents the conditions that were considered in this thesis. For studying the thrust frame and the fuselage in the aft skirt, the main forces that should be considered for a first analysis are the thrust and the weight of the vehicle as well as the location of both vectors. The origin of the reference system is located at the nose cone and the negative axis of the vertical coordinate, which is considered to be the *z* component, points towards the centre of the thrust frame. In this case study,the mass of the rocket, as the sum of all its components is 997.021 kg, and the centre of mass of the rocket is -3.64 m given by equation 4.1,

$$z_{cm} = \frac{1}{M} \sum_{i=1}^{N} m_i z_i \tag{4.1}$$

where M is the total mass of the rocket, N is the number of components and m_i and z_i are the mass and the location of each component, respectively. All these values were obtained from previous assumptions done by CEiiA. The point where the thrust is applied is also crucial for the study that will be described in the following sections and, an initial estimation was provided by CEiiA, with a *z* coordinate value of -5.251 m. Finally, the thrust is represented based on the following description in the CEiiA's documents. "Thrust is applied to the thrust frame on the TVC's (thrust vector control) pivot point, over an arbitrary area. Such an area projects a circle 0.200 m in diameter and centred on the vehicle's axis. The pivot point is located on the vehicle's axis, 0.128 m from the lowest point of the thrust frame. The

TVC angle (β) is measured against the vehicle's axis." Finally, it is considered a force of 25250 N for the thrust with 8° of TVC.

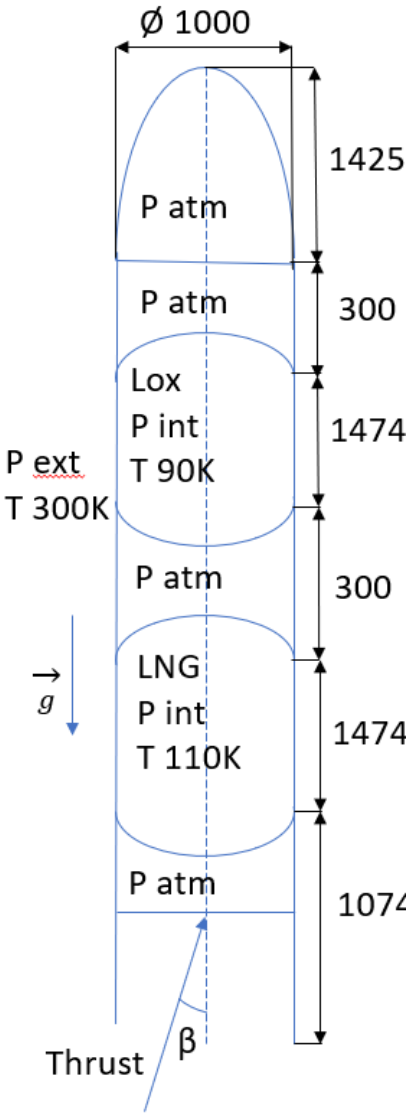

Figure 4.1: Representation of Morpheus' operation loads and its dimensions in mm (not in scale)

4.2 Finite Element Analysis

In this section, a description of the FEM analysis is going to be detailed for the thrust frame and the aft skirt. In both of these models, since this was a preliminary analysis of the rocket components, it was performed an analysis with 2D elements which is representative of the reality while achieving the results with low computation effort and in a short time. As a result, the model was first changed to its middle surface, using the "Midsurface by Face Pairs" option of the CAE software, to allow the usage of the 2D elements option.

4.2.1 Thrust Frame FEM

The analysis of this Morpheus's component started with a model with 3 holes with 8 mm in diameter that would connect to the aft skirt, and two holes to pass the tubes from the fuel and propellant that would connect to the motor itself. Since this is a first model, all the other supports that are needed to fix the motor are not represented and there is no reinforcement in any of the holes, but this simpler model is enough for a first iteration to get an approximation of the final results. This representation is shown in figure 4.2. However, this model shows a high stress concentration in the holes near the edge, which would connect to the aft skirt.

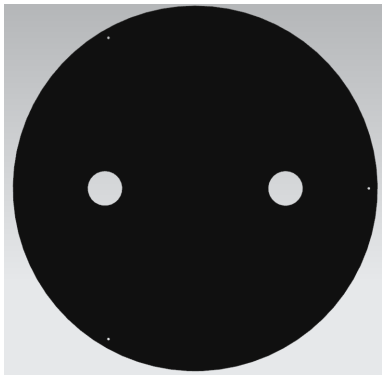

Figure 4.2: Initial model of the thrust frame with 3 holes with 8 mm in diameter

So, to avoid too much stress concentration near the holes, the number of holes was increased to 12 and the diameter was also increased to 12 mm. Also, it was defined a localized area in the vicinity of each hole, where the mesh is more refined for improved accuracy of the solution. This circle allowed for a more detailed study of the region near the holes with more elements which resulted in a better representation of the reality. Similarly, it was defined a circle with 200 mm in diameter in the center of the thrust frame to simulate the thrust area as it was referenced before. A more detailed representation is shown in figure A.4.

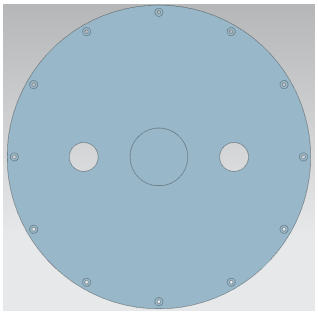

Figure 4.3: Model of the 2D thrust frame with 12 holes with 12 mm in diameter, two holes to connect to the motor and the area for the thrust

After having the complete 2D model with the areas that are necessary to the analysis, a meshing method was done using ”CQUAD4” elements with 10 mm in size and using the ”paver” option as the meshing method. As for the area surrounding the holes, a mesh control was applied with 24 elements on the edge, figure 4.4.

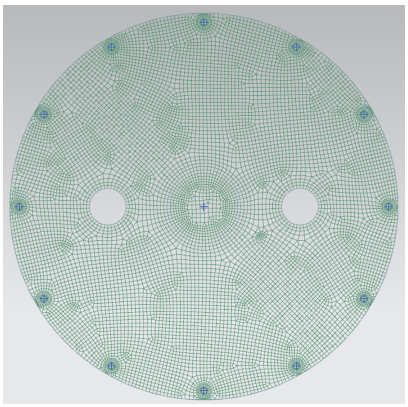

Figure 4.4: Mesh of the final thrust frame model

Now, it is important to understand the connection elements. These elements are used to simulate the screws through the holes, the connection to the mass or the thrust. From the many types of connection elements, the ”RBE2” and ”RBE3” were the elements chosen for this purpose. RBE2 elements are considered rigid elements because they do not allow for relative movement between different nodes. On the other hand, RBE3 elements allow for relative movement between different nodes and this type of element connection distributes the applied force according to the distance between the center of gravity of the group joint and the nodes. As for the moment in RBE3 elements, this is not applied as a moment to the nodes, instead, forces in different directions are applied to the node derived from the moment at the center of gravity, as is shown in the schematic example of figure 4.5.

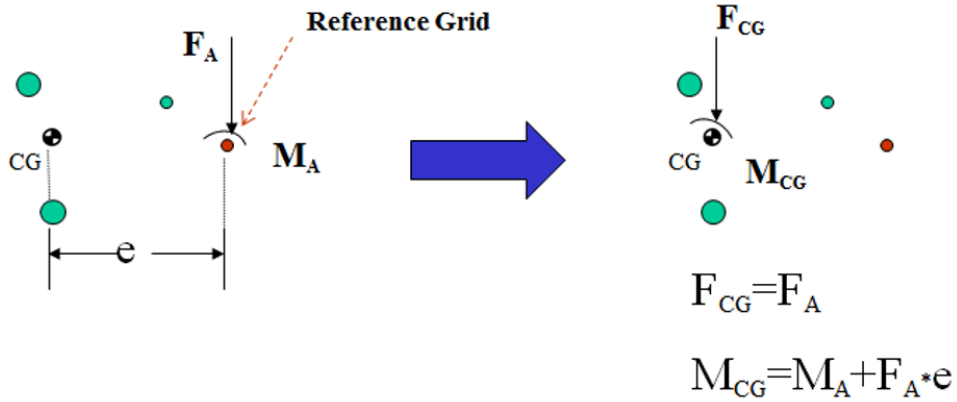

(a) Step 1

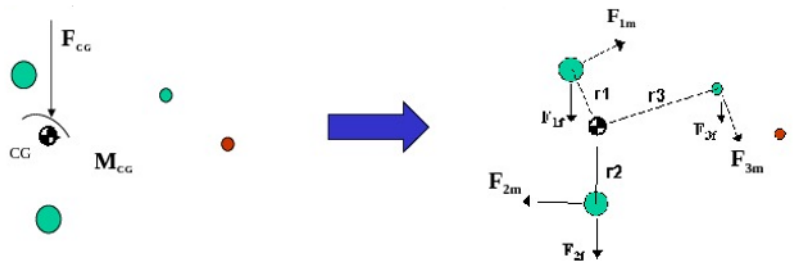

(b) Step2

Figure 4.5: RBE3 element connection mechanics [24]

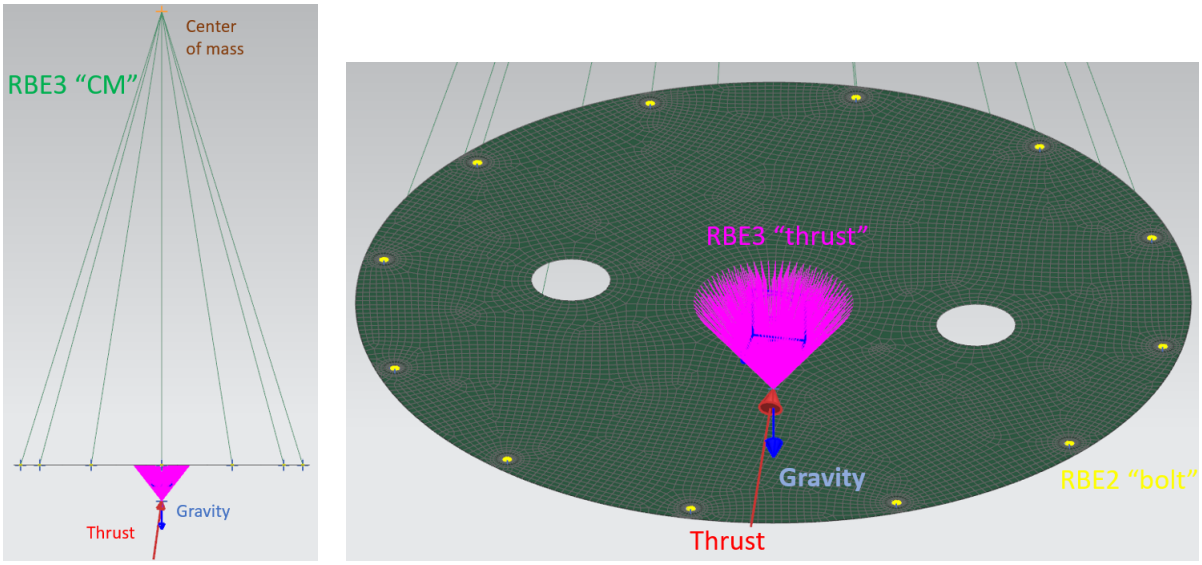

(a) (b)

Figure 4.6: Applied forces and RBE connections

For the thurst frame model, a RBE2 connection was used to design the bolt that is going to be present in the smaller holes, because the bolt is a rigid element that should not allow for any relative movement between different nodes of the hole. However, RBE3 elements are used to connect the holes to the center of mass of the rocket and from the area at the center of the thrust frame to the point where the thrust is applied. This is a more conservative approach that does not transmit any rigidity from the structure of the rocket while also allowing the relative movement of the nodes. Besides that, the only forces applied to this simulation are the rocket's weight and the thrust with an inclination of 8° with the vertical axis, where the gravity is applied. To simulate the weight of the rocket, a CONM2 element with 997.021kg was used at the center of mass and, with a mass distribution using the option ”total for mesh, equal distribution”.

Finally, it was used 2 different types of mesh collectors. A ”laminate” option to simulate the CFRP composites and the honeycomb mentioned in section 3.2. As for the aluminium, the ”PSHELL” was the selected option. The selected options for the ”laminate modeler” are shown in figure 4.7. For the ”PSHELL” properties, the options for ”Use Material 1 for Material 2” and ”Use Material 1 for Material 3” were both selected. These options guarantee that material 1, which is the Aluminium 2219-T851 with the properties of section 3.2, is used as the bending and transverse shear material.

Before simulating the design of the composite and optimizing the solution a few considerations needed to be attended first. To start with, a core was created with the honeycomb properties that were shown in section 3.2. Then, since the optimization of the design was made through experimentation with different thicknesses and angles, and is not possible to try out every single combination, some conditions were previously defined. Each CFRP ply has a thickness of 0.25 mm and the total thickness of the CFRP laminate is chosen by adding or removing fiber plies. Also, the angle of the fiber orientation was chosen to optimize for the structural performance. These angles varied by 15 degrees in each trial. Finally, the core was considered as just one ply and its thickness could vary by 1 mm in each trial.

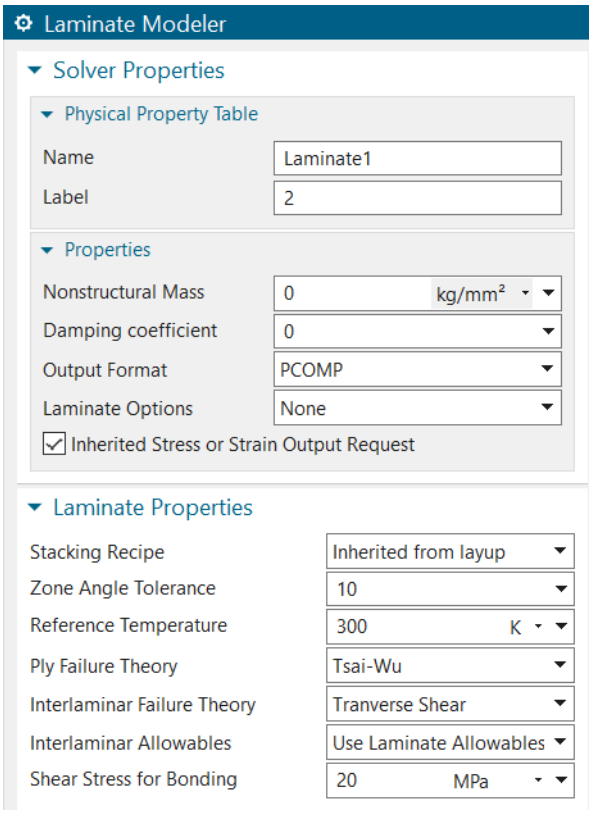

Figure 4.7: Options for the ”laminate modeler” for a mesh using composite materials

4.2.2 Aft Skirt FEM

To start with, the aft skirt was first modelled based on some previous assumptions. There should be 12 holes that would connect to the thrust frame and each one with 12 mm in diameter. It is also important to note that the region under these holes is only a fuselage cover and it is not expected to resist any structural loads. In the upper part of the aft skirt, there are also 12 holes that will be used to join the aft skirt to the y-ring of the fuel tank. These holes were also considered to have 12 mm in diameter to minimize the stress concentration. Between the upper region and the area of the thrust frame, there is a door to allow a quick access to the inner part of the rocket. This door would be screwed to the aft skirt in 8 holes, but after a preliminary analysis of the stress and also a buckling analysis it was concluded that more holes would be necessary. The final model of the door has 28 holes with 8 mm in diameter, figure 4.8. A more detailed representation is shown in figure A.5.

Then, this solid model was transformed into a surface as it was also done for the thrust frame, figure 4.9. For the aft skirt, some important features were studied which required some special details when considering this surface model. There were considered columns that would reinforce the structure of the aft skirt from the top holes to the bottom holes, except for the holes that are present in the middle of the door. The objective of these columns is to prevent the failure not only from the stress that could cause the failure of the structure but also from the buckling which could be a critical factor in this component of the rocket. Besides that, it was also created a circular region in the upper part of the aft skirt to simulate the y-ring which would give a structural reinforcement to the structure. Furthermore, the lower part of the

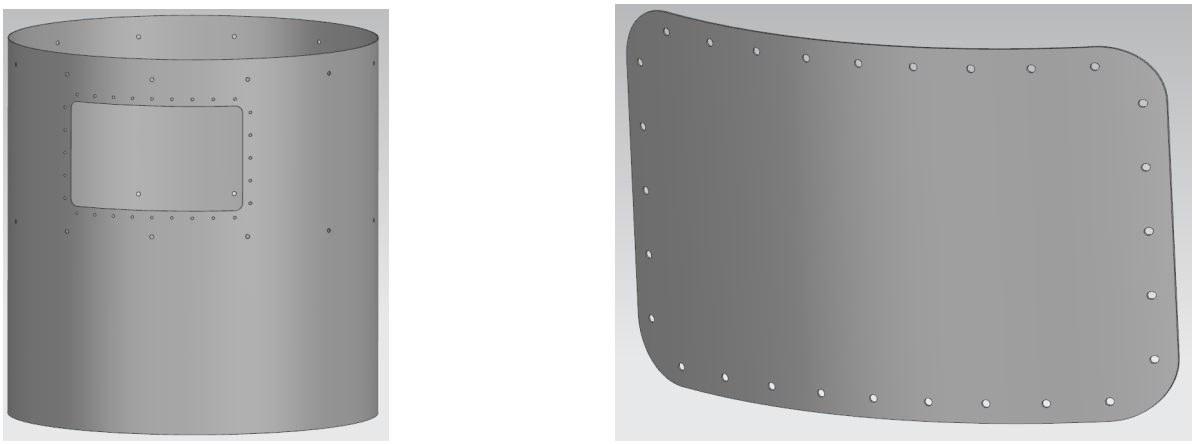

(a) (b)

Figure 4.8: (a) Aft skirt model (b) Door model

aft skirt was separated from the area of the thrust frame, because this lower region is not a critical area of the rocket regarding the impact of the applied loads. This lower part does not need as much material as the other areas which could save weight while guaranteeing the desired performance. Finally, as was the case in the thrust frame, it was defined a localized area in the vicinity of each hole, where the mesh is more refined for improved accuracy of the solution. In addition, these circular regions surrounding the holes allowed for a better visualization and analysis of the results. However, this region should have a reinforcement due to the high concentration of stress near that region. Due to this reason, and to have a good estimation of the reality for the rest of the component, the area surrounding the holes was not considered, that is if this area had a failure index above one the overall component was still considered safe.

For this model, two different 2D meshes were created, one for the aft skirt itself and another one for the door. For both meshes, it was selected ”CQUAD4” element types with the ”paver” meshing method. However, the ”automatic element size” was used to determine the size of the elements which resulted in different sizes. For the aft skirt, it was used elements with 25 mm and, for the door a lower size of 10 mm was chosen. These sizes are slightly lower than the size recommended by the ”auto size” tool, to reduce some errors and to have more accurate results. Besides that, a mesh control was used for different regions of the aft skirt and the door, mainly for the areas surrounding the holes which due to their geometry and concentration of stress required more elements. For the mesh control, it was used two different tools of the *NX Siemens*, the ”number on edge” and ”size on face”. The mesh controls are indicated in orange in figure 4.10.

After that, all the connection elements were introduced, which in this model only corresponded to RBE2 elements, figure 4.11(a). The RBE2 elements that connect to thrust (4.11(a) in yellow) and the RBE2 elements that connect from the upper holes to the center of mass (4.11(a) in blue) were chosen to provide some additional rigidity to the model, which RBE3 does not provide. Although this estimates a better than expected scenario, it is closer to the reality than an RBE3, since there must not be any significant relative movement between these holes, which otherwise could cause a catastrophic failure.

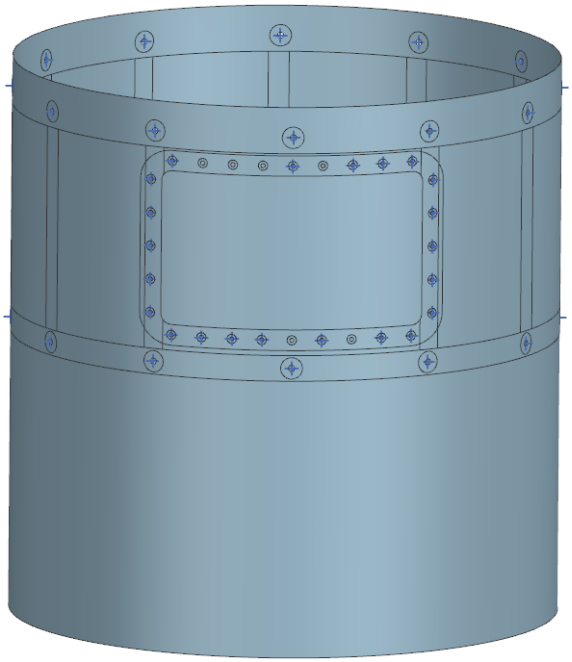

Figure 4.9: Surface of the aft skirt model

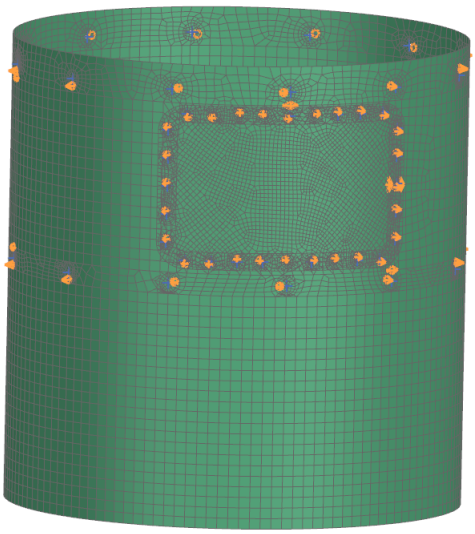

Figure 4.10: 2D mesh for aft skirt and the mesh controls used in orange

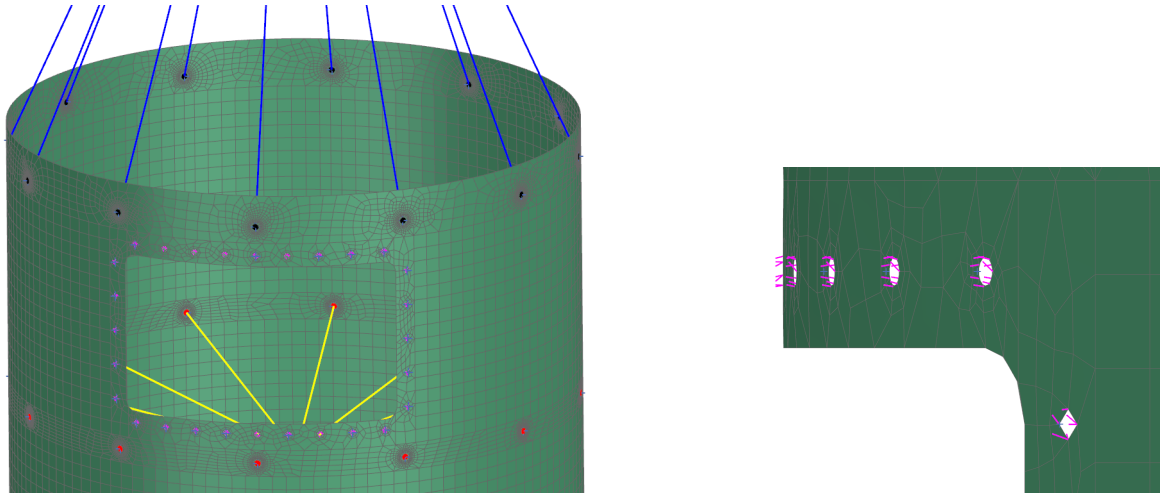

(a) (b)

Figure 4.11: (a) RBE2 connections in aft skirt (b) Detailed RBE2 connection from the aft skirt to the door

Moreover, both the y-ring, which is connected to the fuel tank, and the thrust frame provide the rigidity, which was intended to be simulated by the RBE2 elements. As was the case in the thrust frame model, RBE2 elements were created in the holes of the upper region (4.11(a) in black) and the thrust frame's region (4.11(a) in red). These elements simulate the bolt connection. Finally, for the remaining connection of the door to the aft skirt, RBE2 elements were also used, as is shown in pink in figure 4.11(b). This connection guarantees that each hole of the aft skirt is connected to the hole of the door, while allowing for relative movement between different holes.

Finally, as was the case in the thrust frame, here, the weight and the thrust is applied in the same direction and orientation as described in the previous model. The concentrated mass is also simulated through a CONM2 element with 997.021kg at the center of mass, again, following the same procedure as in the previous example.

For this model, the same options for the simulation of the composite or aluminium materials were done in the same way as the thrust frame (section 4.2.1). Not only the selected options were the same, but also the conditions and methodology used.

There is another important consideration that must be considered which is the integration of the different sections that were previously defined. For example, since the upper region has an extra aluminium part where the Y-ring is located and the part underneath does not have, it must be guaranteed that both parts are aligned in the exterior part of the aft skirt and not in the middle or the interior. So, a "Top" layup offset was selected, with a material orientation starting in the last ply. After all this, the description of the layup must also coincide between layups of different regions, if they are supposed to be in the same plane, which is defined in the layup modeler of the *NX Siemens*, figure 4.12.

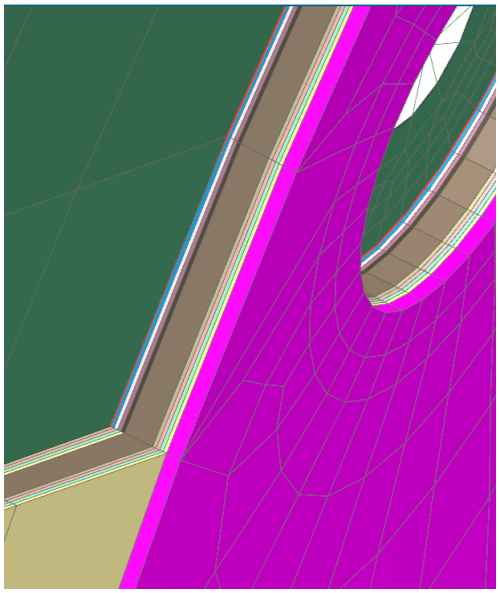

Figure 4.12: Example of the laminate offset, with an aluminium part in pink, and the layers of the composite aligned

Chapter 5

Results and Discussion

In this chapter, it will be described the simulations and the respective results for both the thrust frame and the aft skirt until the final design is obtained.

5.1 Thrust Frame Results

The solver that was selected to analyse the results for either the laminate model or the aluminium one was the ”Simcenter Nastran” with a structural analysis. As for the type of solution, the ”SOL 101 Linear Statics - Global Constraints” was the choice made from the available solution in *NX Siemens*. The ”Inertia Relief” option was also selected to simulate the unconstrained structure in a static analysis. This option is usually used for aircraft in flight, or rockets in space since they are not attached to the ground.

5.1.1 Thrust Frame - Sandwich composite Results

For the laminate results, the stresses of the ply were calculated at the bottom, middle and top of each ply and the Tsai-Wu method was used for all the directions of ply failure (”11”, ”22”, ”33”, ”12”, ”23” and ”31”) except for the core where a core shear method is used. A factor of safety of 1.42 was also introduced, as explained in section 2.3.

After that, it was important to define a method to optimize the results. The methodology used is as follows:

1. Start with a 20 mm core
2. Obtain the minimum number of CFRP plies, with a sequence of [0° ,$+45^\circ$], until the failure
3. Reduce the thickness of the core until failure
4. Calculate the final weight
5. Increase the initial thickness of the core by 10 mm and repeat the process from point 2 through 5

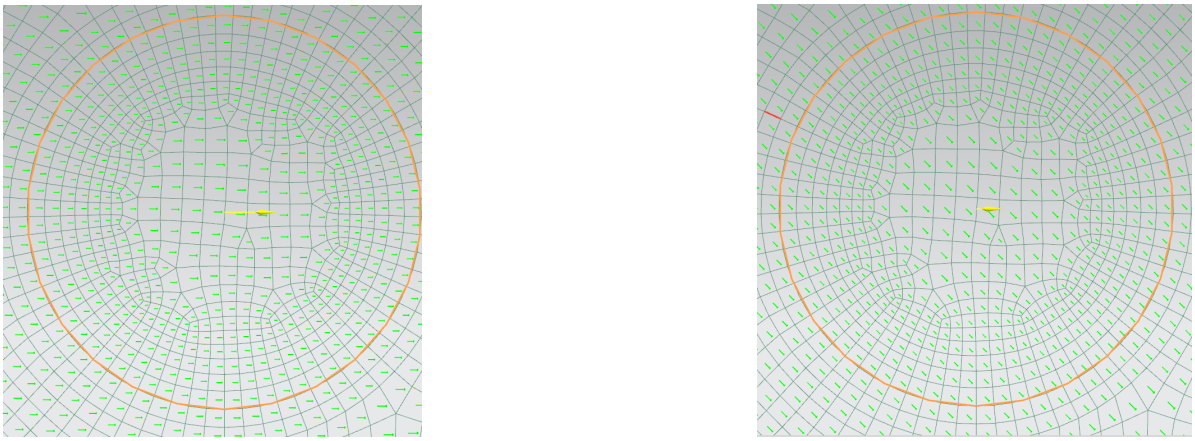

(a) (b)

Figure 5.1: Thrust frame fiber orientation (a) 0° (b) 45°

The fiber orientations of the CFRP used in the thrust frame model are shown in figure 5.1.

After following these steps, a minimum weight was found with a core of 29 mm and 6 CFRP plies of 0.25 mm on each side, as it is shown in Table 5.1.

Table 5.1: First optimization for a composite thrust frame

Core [mm]	**CFRP skin (one side) [mm]**	**Mass [kg]**
20	3.75	9.88
29	1.5	6.24
34	1.25	6.27

However, it was still possible that the minimum weight possible could be obtained for a higher number of CFRP plies, and subsequently a lower core thickness. So, to optimize the results even further, this was tested and the results are shown in Table 5.2.

Table 5.2: Final optimization for a composite thrust frame

Core [mm]	**CFRP skin (one side) [mm]**	**Mass [kg]**
29	1.5	6.24
24	1.75	6.21
22	2	6.5

Finally, a thrust frame with a core of 24 mm and 7 plies of CFRP provides the lightest thrust frame possible that can withstand the forces to which it will be subjected to. In Appendix A, it is shown a complete description of the maximum stresses in all directions as well as the maximum failure index for the thrust frame, Table A.6. It should also be noted that the failure index should be below 1 to guarantee that there is no failure.

After analysing figure 5.2, it is clear that the maximum point of failure index is located in a region of the right hole that will connect to the motor. The region surrounding the holes was not considered in the next section for the aft skirt as it will be further explained, however here it was considered due to several reasons. First of all, this is a hole with a large diameter and the weight of the motor was not considered in this simulation. This is also a component that will experience severe vibration during launch and that

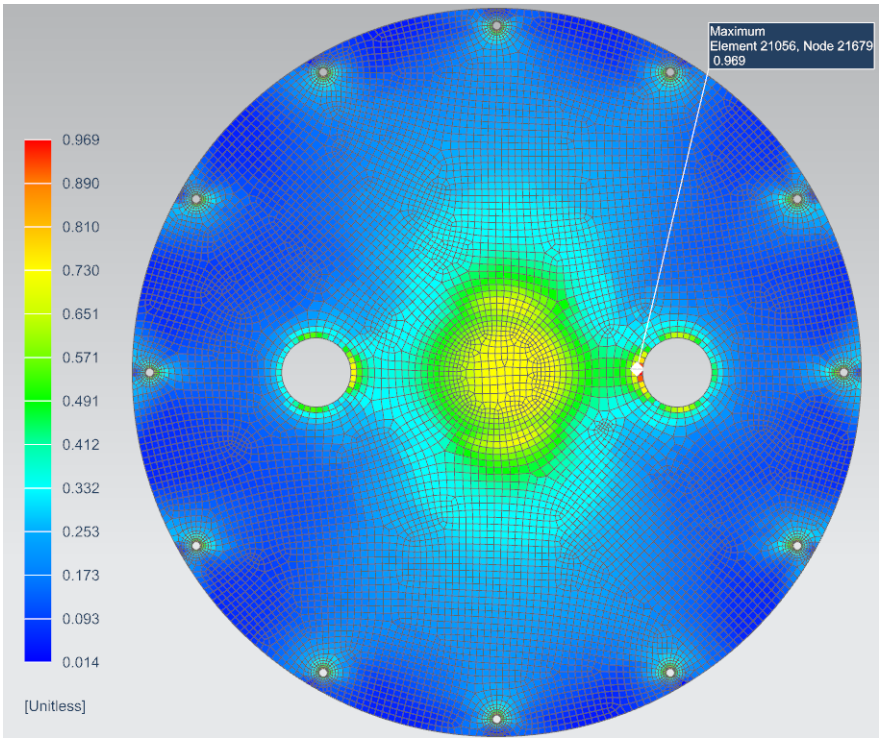

Figure 5.2: Maximum failure index (elemental-nodal) for the final thrust frame with 24 mm of an aluminium honeycomb's core and 7 plies of 0.25 mm CFRP on each side

was not simulated as well. Then the connection of the motor to this support was not clear at this point with possible changes to the design in the future. Due to all these reasons, and because the results were obtained for a factor of safety of 1.42, this point of failure was considered during the process of achieving the best design possible. However, this is a region that should be reinforced in the future, in more detailed models, which would reduce the stresses at that point. The same is also true for the other holes because these regions usually concentrate a lot of stress and because of that, it is important to reinforce those areas. This could lower the mass of the thrust frame even more since it would allow for a decrease in the core's thickness and/or the number of CFRP plies of the overall structure, while only increasing the area surrounding the holes. However, this was not studied at this point because it would require a much more detailed analysis which does not make sense at this early point of the development. And, also because in this way we are providing some margin of safety to the model since a reinforcement would provide additional strength to the model, reducing the risk failure.

Finally, the same optimization was done for the other 2 types of HexWeb® Aluminum Flex-Core® honeycomb [20] with the 5056 alloy and a cell count of F80 which correspond to a density of 4.3 pcf and 6.5 pcf. The comparison between these 2 honeycombs and the one previously used is shown in Table 5.3. Although these two last honeycombs with a lower density result in a lower mass for the thrust frame, the core thickness must be kept under 25 mm to avoid the problems already mentioned before. In conclusion, since these two honeycombs do not satisfy the requirement for the honeycomb thickness, the honeycomb with a density of 8.0 pcf is considered the best choice for a composite thrust frame.

Table 5.3: Results of the final optimization for 3 different honeycombs

Honeycomb description			Simulation results			
Aluminium alloy	**Material/Cell count - Gauge**	**Nominal density [pcf]**	**Core [mm]**	**Fiber carbon ply (one side) [mm]**	**Total thickness [mm]**	**Mass [kg]**
5056	F80 - 0.0014	4.3	56	0.75	57.5	4.84
5056	F80 - 0.0020	6.5	34	1.25	36.5	5.57
5056	F80 - 0.0023	8.0	24	1.75	27.5	6.21

5.1.2 Thrust Frame - Aluminium Results

After optimizing for the composite thrust frame, the next step was to optimize the aluminium thrust frame. To optimize the thrust frame, the thickness was increased by 1 mm each time until the von-Mises stress was lower than the ultimate tensile strength. The minimum thickness which allowed this criteria to be fulfilled was 10 mm which corresponded to a mass of 24.11 kg.

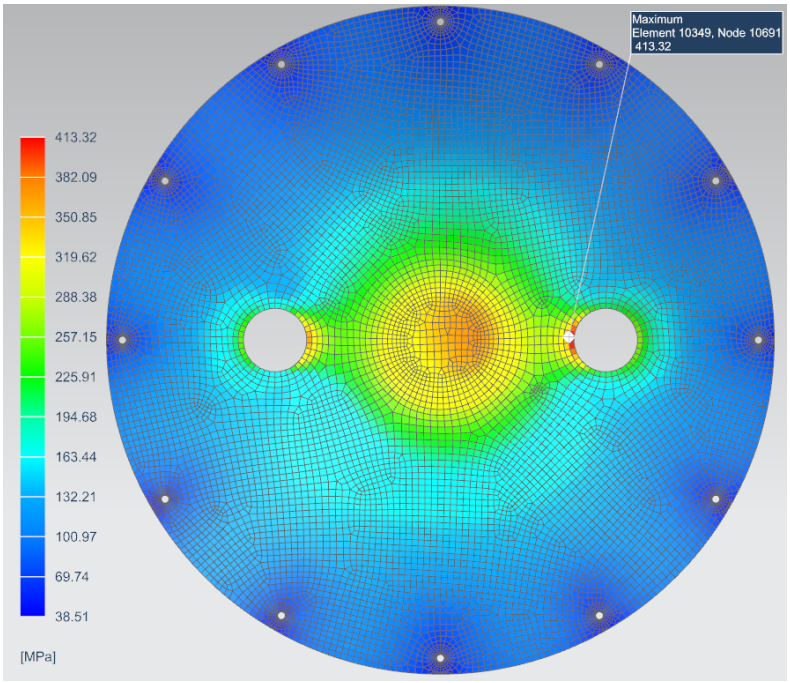

Figure 5.3: von-Mises stress (elemental-nodal) for a 10 mm aluminium thrust frame

5.1.3 Thrust frame - CFRP results

Lastly, the thrust frame was also tested using only CFRP. For this model, 63 plies must be arranged in a sequence of $[0°/45°]$ to resist to the applied loads, which corresponds to a total thickness of 15.75 mm. The total mass for this model is 16.18kg, which is much more than the model that considers the honeycomb in the middle of the carbon fibers. Besides that, this is not feasible because it requires too many plies which could cause problems in the manufacturing process, since an increase in the number of plies would increase the probability of small defects in the plies, as well as the cost.

5.1.4 Thrust Frame - Final Results

To sum up, Table 5.4 shows the final results for the different designs. In this table it is clear to notice the combination of the CFRP skin with the honeycomb results in the best design possible. The only drawback that could be considered is the thickness. However, this is not a concern for this application. Nevertheless, as was already stated before, the high thickness of the honeycomb could be problematic and the difference in weight does not justify that increased risk. So, the model with CFRP and honeycomb 8.0 is the best possible design that was achieved with these materials and should be considered in more detailed studies in the future.

Table 5.4: Final results for the thrust frame

Material	Carbon thickness (one side) [mm]	Core thickness [mm]	Total thickness [mm]	mass (kg)
CFRP + Honeycomb 8.0	1.75	24	27.5	6.21
CFRP + Honeycomb 6.5	1.25	34	36.5	5.57
CFRP + Honeycomb 4.3	0.75	56	57.5	4.84
Aluminium	—	—	10	24.11
CFRP	15.75	—	15.75	16.18

5.2 Aft skirt Results

The objective of this section is to arrive at the best possible design not only for the aft skirt but also for the door. Although only a static analysis was done for the thrust frame, the same is not enough for the aft skirt. For this component of the rocket, it is important not only a static analysis but also a buckling analysis. It is possible to compare the structure of the aft skirt to a cylindrical column that is being compressed on both ends. In the case of the aft skirt, the compression occurs in the top part due to the weight of the rocket that is above it, and from the bottom part because of the thrust that is being applied. These forces can cause a loss of stability that leads to a buckling failure. So, a buckling analysis will be simulated after a final model is obtained from the static analysis.

Firstly, for the static analysis the same options, available in *NX Siemens*, that were used for the simulation of the thrust frame were also selected for the aft skirt since there are no significant changes between these components regarding this analysis. These options were already mentioned before in section 5.1. The simulations for the static analysis did not consider a factor of safety during the analysis, but it was considered in the final design, which has the factor of safety required.

On the other hand, for the buckling simulation, it was also used the solver of ”Simcenter Nastran” with a structural analysis. However, it was selected the solution type of ”SOL 105 Linear Buckling”. In contrast with the static analysis, for the linear buckling, it is not possible to select the ”inertia relief” option. So, to analyse the aft skirt and the door itself for the buckling case, it was necessary to fix the concentrated mass to have the minimum constraints necessary. The mass was chosen for this because in the initial moments of the launch we can consider this point as fixed in space and, also, because this would be the most conservative approach since there were other tests done but this option resulted in

the worst-case scenario. Besides that, all the applied forces are the same as in the static analysis. It was also considered the FOS of 1.42.

5.2.1 Composite aft skirt - Static analysis

First of all, it should be noted that the model of the aft skirt has a lot of different combinations possible and, because of that a sequential analysis process needs to be considered. In the first simulations, it was clear that the lower part of the skirt was not a concern regarding the possibility of a failure caused by the applied forces. Accordingly, the lower part of the skirt was tested with only 3 plies of CFRP and, yet, this region still was not the point of failure. It was possible to reduce even more the number of plies which would, correspondingly, reduce the weight. However, this test was not continued further because, with just 3 plies, which equals to 0.75 mm of thickness, other problems start to emerge besides the failure caused by the stress. For example, the high temperature that this region needs to withstand due to the hot gas that is being expelled could lead the plies to start melting. So, the lower part of the aft skirt should require a thermal reinforcement to prevent this situation. To attach this thermal reinforcement to the plies, a minimum thickness is necessary and to maintain a realistic model, the thickness of this part was kept at 0.75 mm, corresponding to 3 CFRP plies in all the subsequently simulations. Nevertheless, a more detailed study should be done in future works.

In this model, two different components are being considered, the aft skirt itself and the door. By analysing these two components simultaneously the point of failure was many times present in the door, which did not allow for the optimization of the aft skirt itself. Therefore, the door was removed from the simulation and, instead, multiple RBE2 from the edge of the opening of the door were connected to the center of this area as is shown in figure 5.4. In this way, it was guaranteed that there was no relative movement between different points in the edge. This increased the rigidity of this region more than the door could because the RBE2 elements have an infinity rigidity, but this is a good approximation and, after optimizing the aft skirt, the door is going to be again introduced to make sure that the approach taken by using the RBE2 was a good consideration and that the complete structure can resist all the applied forces. Besides that, as for the CFRP orientation, the plies were simulated based on a sequence of $[0^\circ/45^\circ]$ as shown in figure 5.5.

For the next step, the impact of the aluminium column was studied. For this, a ring of aluminum with 3 mm of thickness in the y-ring region was kept constant. Then, five CFRP plies were added to the rest of the aft skirt, except for the lower part as explained before, also it was added 2 mm of aluminium to the columns. This configuration resulted in several failure points, and, for this reason, the column thickness was reduced to 1 mm and one more CFRP ply was added to test which of the following options is the better one: increasing the number of CFRP plies or increasing the thickness of the columns. By doing this, the weight was reduced by 0.01 kg, from 7.57 kg to 7.56 kg, and not only that but the failure index was also reduced which indicated that an increase in the number of plies is the better option. Finally, as a final consideration, the aluminum was completely removed from the columns and the number of carbon plies were increased to seven. This configuration is not only lighter with 7.54 kg but also did not

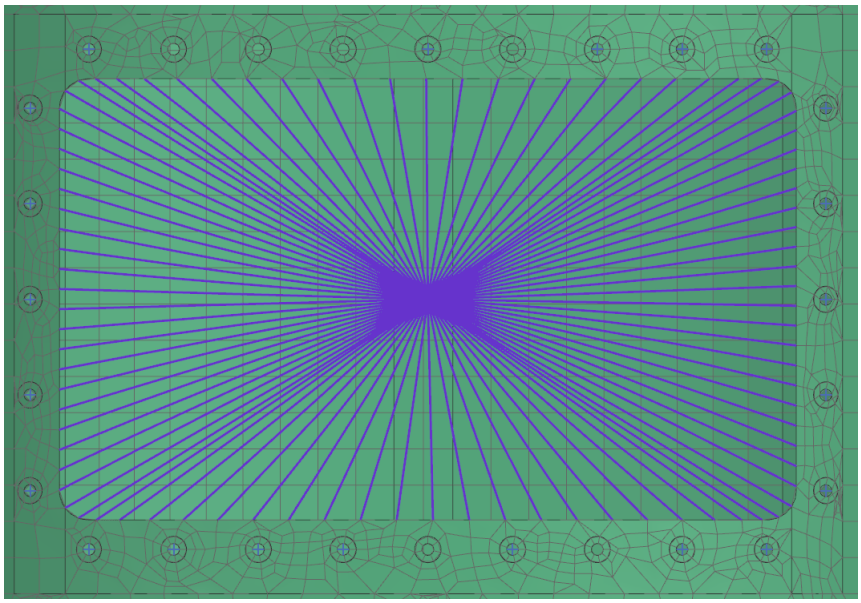

Figure 5.4: RBE2 elements replacing the door

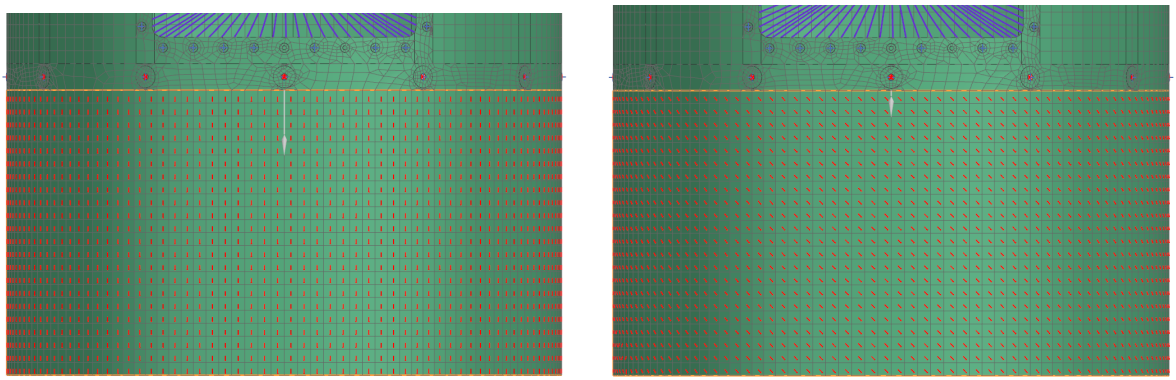

(a) (b)

Figure 5.5: Aft Skirt fiber orientation (a) 0° (b) 45°

have any points of failure in this static analysis. After that, one ply was removed to test if the structure could resist the loads while allowing for a reduction in the mass, but this was not the case, and the new structure had multiple failure points. According to these results, figure 5.6 the columns do not provide any increase performance for the structure, so they were not considered anymore.

Following this, the thickness of the aluminium that represents the y-ring was tested. At this point, the lower part of the aft skirt was still being modelled with just three plies and without aluminum columns. Firstly, the ring's thickness was decreased to 2 mm while one ply was added. This model could resist all the loads and it had a mass of 7.19kg. After this, the ring's thickness was reduced even more to just 1 mm, while one more CFRP ply was added, which resulted in a total weight of 6.83 kg. Consequently, the next approach was to completely remove the y-ring, while, again, adding one more CFRP ply to the aft skirt. However, this design had several points with a ply failure index above 1 which indicates a failure in the structure. Finally, at this point, the conclusion was that a y-ring with 1 mm of aluminium provided the best design possible. However, the CFRP plies could be reduced even more. So, two more tests were

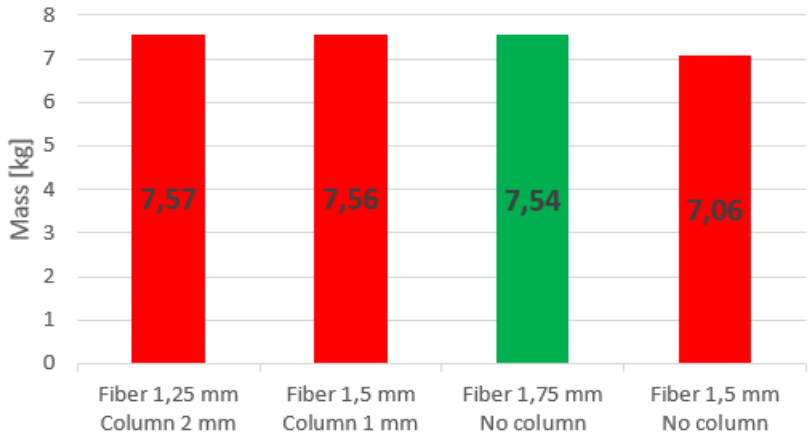

Figure 5.6: Weight of the aft skirt when testing for the aluminium column. The color red indicates the failure of the structure, while the green color corresponds to a safe model

done, one with 8 CFRP plies (2 mm) and another with 7 CFRP plies (1.75 mm), but only the former one could resist all the applied loads. As a result, the best option, at this stage, was the model with 2 mm of CFRP in the aft skirt, and, 1 mm of an aluminium y-ring, figure 5.7.

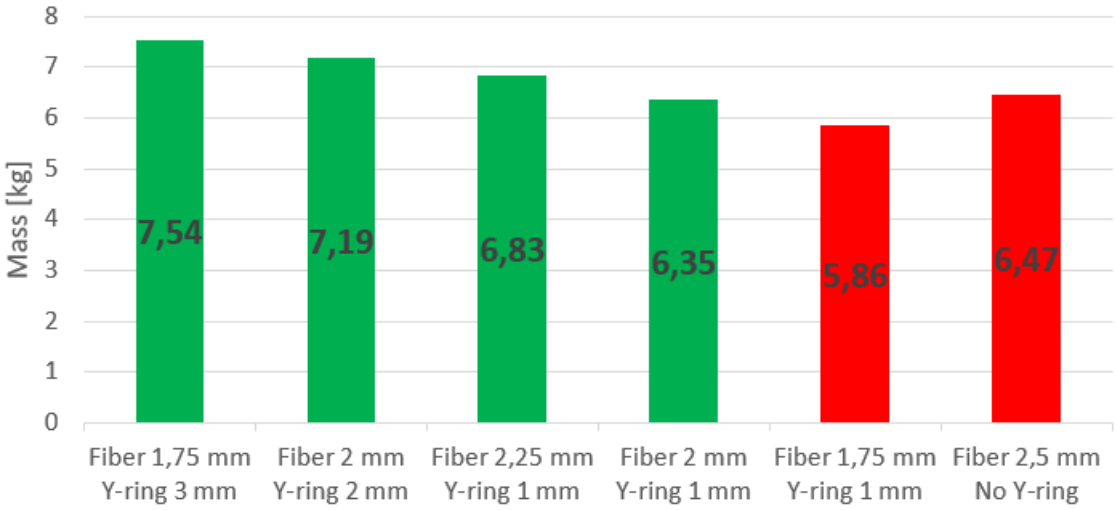

Figure 5.7: Weight of the aft skirt when testing for the aluminium y-ring. The color red indicates the failure of the structure, while the green color corresponds to a safe model

Finally, the honeycomb aluminium's core was tested. It was added to the aft skirt, except to the lower part of this component. The core was aligned normal to the circular face. In the first test, only 2 mm of core were added with 1 mm of CFRP on each side of the core. However, the simulation of this model showed several failing points. Nonetheless, the core was increased to 6 mm, which corresponded to the maximum core thickness with 3 CFRP plies on each side of the core that resulted in a reduction of the total mass. For this model there were no failures, so, the core was reduced to the minimum thickness that was still strong enough to resist all the loads. This resulted in a final model with 4 mm of core thickness and 3 CFRP plies on each side, resulting in 6.20 kg of final weight, figure 5.8.

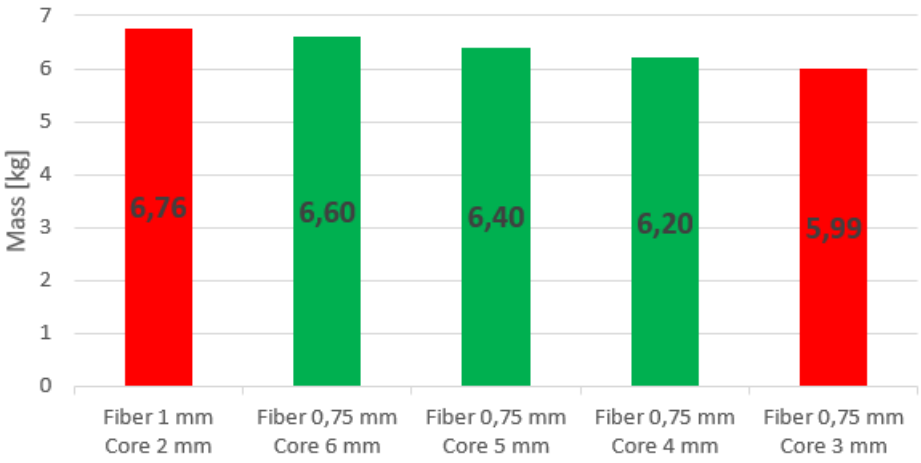

Figure 5.8: Weight of the aft skirt with an honeycomb core. The color red indicates the failure of the structure, while the green color corresponds to a safe model

Although the honeycomb in the middle of the fuselage of the aft skirt could save some weight, this is a small difference that does not justify the difficulty in the manufacture. Additionally, it would also increase the cost not only in the manufacture but also in the material itself since this small honeycomb thickness is not a standard dimension and would need to be obtained through a special request with possible implications in the properties of the material itself. Grünewald et al [25] described that 3D sandwich structure like a circular shape can be manufactured, however the more complex the curvature, the greater the challenges in the manufacturing process. Also, the manufacturing imperfections of the core or the interfaces between the skins and the core for cylindrical panels usually fail due to buckling [26]. Besides that, in this case, the honeycomb core is only being applied at the upper region of the aft skirt which would increase the difficulty in the manufacturing process if the aft skirt would be manufactured as one piece. Such increased difficulty would also increase the economic cost which does not justify the small difference in weight of 0.15kg which corresponds to only 2.4% of the total weight of the aft skirt. Due to these reasons, the study of the aft skirt was continued with 8 CFRP plies in the upper region of the aft skirt.

After this, the RBE2 elements that were simulating the door were replaced for the door itself, and the door was connected to the aft skirt through RBE2 elements as was explained in 4.2.2.

Firstly, a door made out of only CFRP plies was tested. The first design consisted of an 1 mm thickness door, but this model failed not in the door itself but in the aft skirt. Then, one more CFRP ply was added but, once again, the failure point continued to exist and, this time the failure index was even higher. Because of this, the thickness of the door was reduced to 0.75 mm, but the design continued to fail in the aft skirt region. By reducing the number of plies in the door to only two fibers, the failure point started to appear at the door. In conclusion, these results show that an aft skirt with 2 mm is not possible when considering the implementation of the door itself. So, the aft skirt thickness was increased to 2.25 mm which corresponds to nine CFRP plies. In this model, a door with 0.75 mm was proven to be safe with the failure index shown in figure 5.9. In Appendix A, it is shown a complete description of the maximum stresses in all directions as well as the maximum failure index for the aft skirt and door, figure

A.7. For a door with just 2 CFRP plies the door had several failure points which led to the number of CFRP for the door to three. Additionally, due to the increase in weight because of the need to add one additional CFRP ply, and even though, the CFRP modeled was chosen instead of the design with the honeycomb sandwich structure, it was still tested the latter model. However, all the models with 3 CFRP on each side of the core with either 4mm, 5 mm or 6 mm failed when considering the door instead of the RBE2 elements which showed that the CFRP model was the ideal design not only for the manufacturing process but also would result in a lighter model. As a final remark, the model with an aft skirt with 2.25 mm and a door with 0.75 mm has a mass of 6.83 kg and 0.21 kg respectively, which gives a total weight of 7.04 kg for the entire model. Although a factor of safety was not considered during this analysis, this model has almost the factor of safety required, since the maximum failure index corresponds to 0.715, which multiplied by the FOS of 1.42 results in 1.0153.

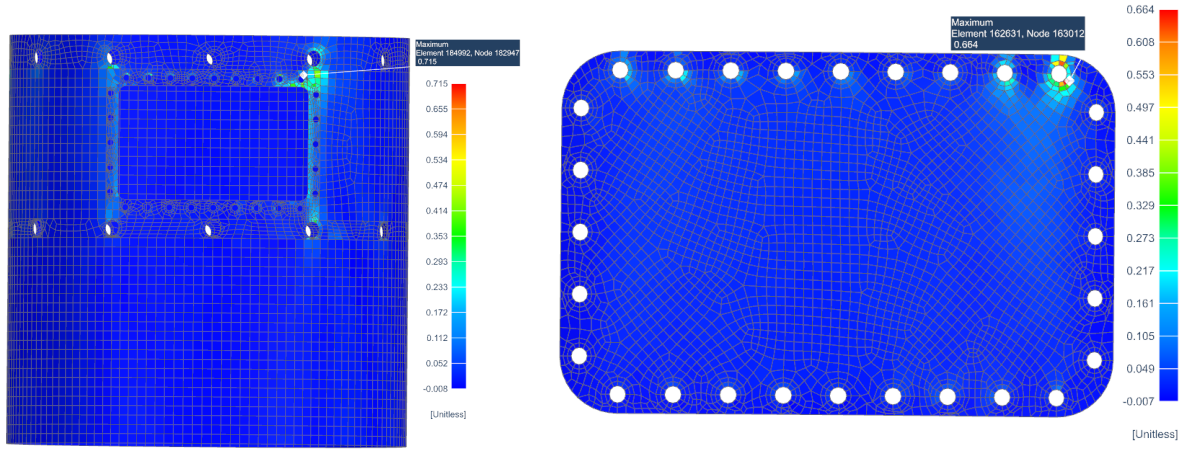

(a) (b)

Figure 5.9: (a) Failure index for the final model of the aft skirt (b) Failure index for the final model of the door

It was also tested a door with a honeycomb core in the middle. However, one CFRP ply on each side of a 2 mm core was the maximum number of CFRP plies and core thickness that resulted in a lower weight than the model with only CFRP plies. Since this model could not withstand the stresses that it was subjected to, this model was not further tested.

Finally, it was considered a door made out of aluminium. For this, the ”PSHELL” option was selected for the door’s mesh with the options described for the aluminium thrust frame in section 4.2.1. In this model, to have a door lighter than the CFRP door, the maximum thickness possible was 0.3 mm. But for this thickness, the door could not resist the stresses since the maximum von-Mises stress was 1247.31 MPa while the maximum allowed is 425 MPa.

To sum up, the design that provided the lowest weight while resisting all the stresses was the one with an 1 mm aluminium Y-ring, a lower fuselage with 0.75 mm of CFRP and the rest of the fuselage with 2.25 mm of CFRP, while the door is made out of 0.75 mm of CFRP.

5.2.2 Aluminium aft skirt - Static analysis

In this section, it is going to be analysed an aft skirt made out of only aluminium, in contrast with the previous section. For this, five different mesh regions were selected which represented the door, the region of the y-ring, the area of the thrust frame, the area between these two last sections and the lower region of the aft skirt below the thrust frame. For all these meshes the element size was chosen by reducing in half the element size suggested by the ”automatic size tool”, except for the lower skirt where it was selected an element size of 25, figure 5.10.

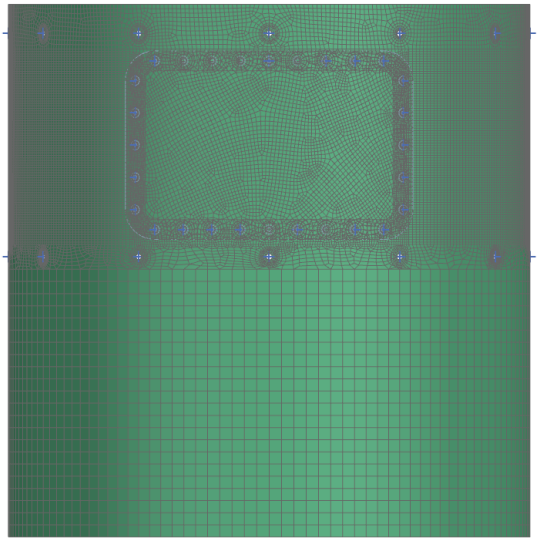

Figure 5.10: Mesh for the aluminium aft skirt

Firstly, for this model, in each iteration was considered changes of 0.5 mm of aluminium. Besides that, all the aft skirt fuselage was modeled with the same thickness, essentially to be easier to manufacture but also because the thickness is too small, and the small changes in thickness between different sections that could decrease the weight of the aft skirt are too small to justify the additional difficulty in the manufacturing process. Additionally, from the results of the previous model, it was shown that the columns did not improve the performance, thus, the columns were not considered for this case. In this way, it is also possible to manufacture the complete aft skirt with just one piece. The manufacture process would start with flat sheets of aluminium, then roll them, and, after having the circular shape, a friction stir welding would be done between both ends of aluminium sheets. Moreover, the y-ring was also simulated in this model, so as to compare to the previous design of section 5.2.1, a 1 mm thickness of aluminium was added to the top region of the aft skirt.

In the next step, the door was considered to be made out of aluminium and it was also considered iterations of 0.5 mm of aluminium each time. In the first simulation, an aft skirt with 0.5 mm of aluminium and a door with 0.5 mm of aluminium were tested. But this model could not resist the stresses that it was subjected to. So the thickness of the aft skirt was increased to 1 mm. This model could resist the stresses since the von-Mises stress was below the maximum allowed of 425 MPa, as shown in figure 5.11. The aft skirt with 1 mm of aluminium and 1 mm of an aluminium ring has a mass of 10.47kg, while the 0.5 mm aluminium door weighs 0.32kg, which combined gives a total mass of 10.79kg.

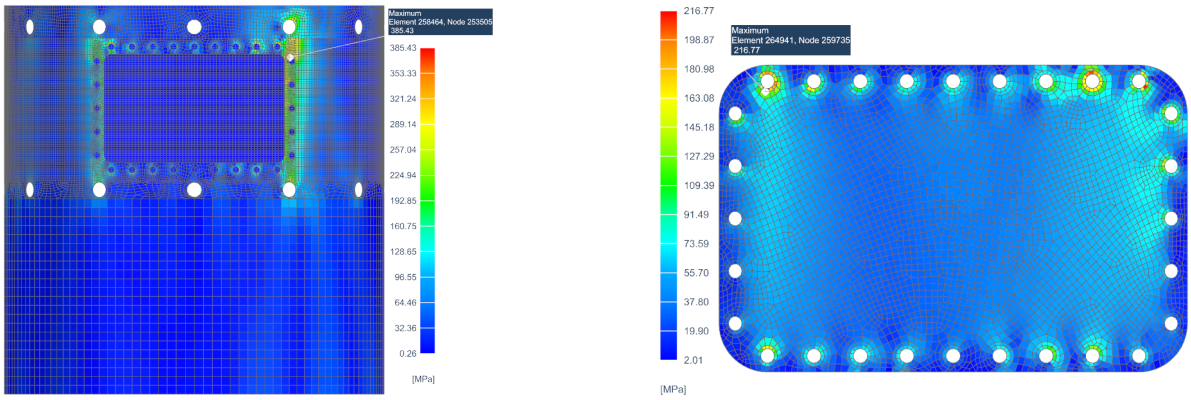

(a) (b)

Figure 5.11: (a) von-Mises elemental stress for the 1 mm aft skirt (b) von-Mises elemental stress for the 0.5 mm door

After this, and for the same aluminium model of the aft skirt, two different models for the door were considered. The first one considered only CFRP for the door. As a result, the minimum number of plies that were needed to withstand the forces is 3 plies which correspond to 0.75 mm of total thickness. This model of the door has 0.21 kg of mass. Then a model with a honeycomb core was considered. For this model, the maximum thickness of the core that had a mass lower than 0.21kg was 2 mm. However, this door with just one ply on each side of a 2 mm thickness core could not resist the stress that it was subjected to.

Finally, since the CFRP door has a lower mass than the aluminium door, the former one should be selected. According to these results, the aluminium aft skirt with a CFRP door has a total weight of 10.68kg. However, the aluminium aft skirt is heavier than the CFRP model which only has 7.04 kg.

5.2.3 Aft skirt - Buckling analysis

For the buckling analysis, if the buckling modes are below 1 the structure would become unstable and fail due to buckling. Therefore, the final design obtained in the static analysis, corresponding to the CFRP aft skirt and door, was tested. However, the first model of this structure had a value of 0.977 in the region of one of the holes of the door, as shown in figure 5.12.

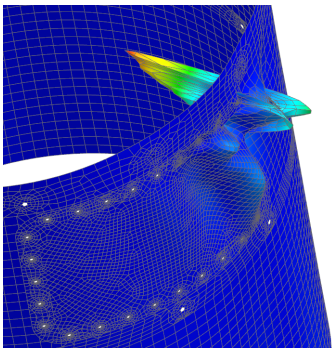

Figure 5.12: Failure of the first mode of buckling (0.977) for a door with 3 CFRP plies

Subsequently, it was necessary to reinforce the door with one more CFRP ply, which corresponded

to a total of four plies and a total thickness of 1 mm. As a result of this change, the first mode of buckling would be 1.18, which is stable. Even though this is close to one, it should be noted that this structure would be reinforced in a more detailed study in the region of the holes. The second and third modes of buckling correspond to 1.25 and 1.54, respectively, and the first three modes are shown in figure 5.13.

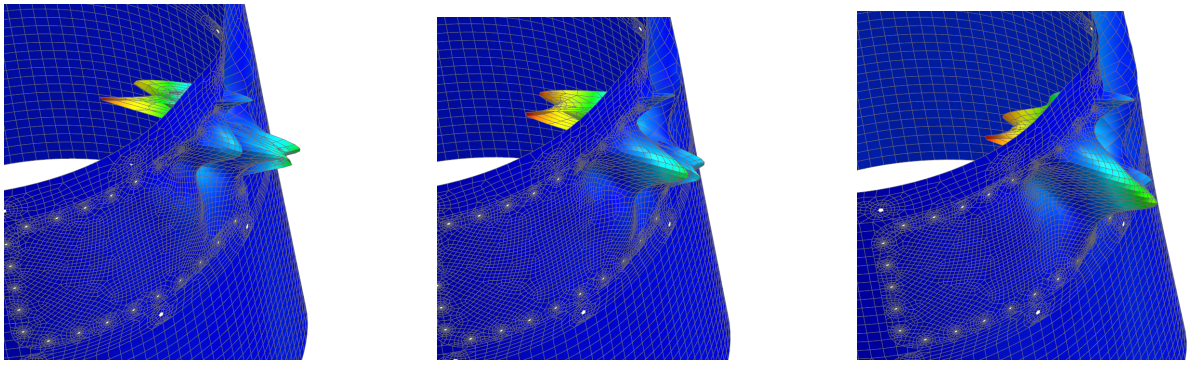

(a) (b) (c)

Figure 5.13: Modes of buckling for the 1 mm carbon door (a) First mode (1.18) (b) Second mode (1.25) (c) Third mode (1.54)

However, these simulations do not take into consideration the factor of safety of 1.42. To consider the additional safety measure required, the door required 4 more CFRP plies. The three first modes of buckling are represented in figure 5.14, and the first mode has a value of 1.59 which is greater than the 1.42 corresponding to the factor of safety.

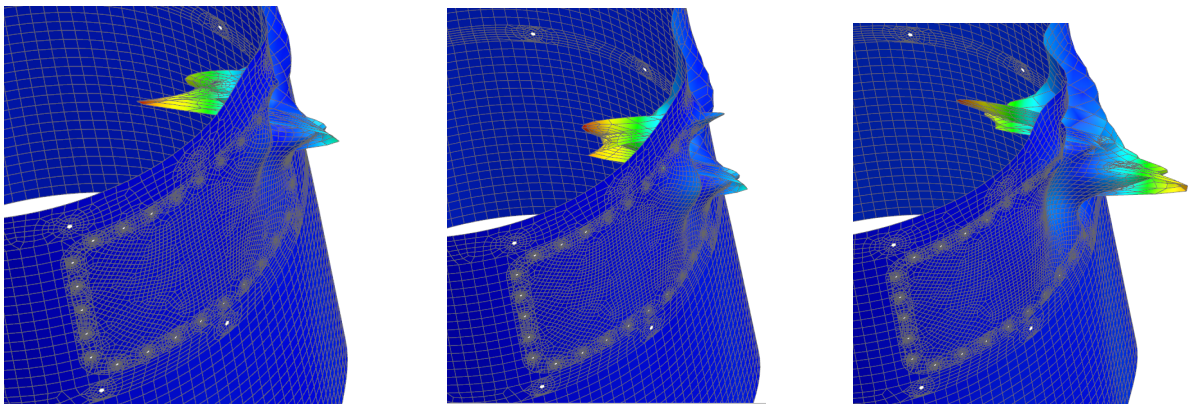

(a) (b) (c)

Figure 5.14: Modes of buckling for the 2 mm carbon door (a) First mode (1.59) (b) Second mode (1.82) (c) Third mode (2.17)

Finally, this corresponded to the final design of the aft skirt and the door. The 1 mm aluminium Y-ring, a lower fuselage with 0.75 mm of CFRP and the rest of the fuselage with 2.25 mm of CFRP, corresponding to a weight of 6.83 kg. Additionally, the final model of the door corresponded to 8 CFRP plies, giving a total of 2 mm thickness and 0.55 kg of mass.

Chapter 6

Conclusions

In this chapter, the final results of the work developed during this dissertation are presented, as well as some considerations for further developments in the future.

6.1 Achievements

The work developed is divided into two main topics: the design of a sounding rocket (Morpheus) and the optimization of two components of the rocket using different materials. Both of these topics were continuously discussed with CEiiA.

Firstly, the general conceptual design of the rocket was studied based on some requirements initially provided by CEiiA to meet the mission requirements. This sounding rocket was named Morpheus and its main objective is to reach an altitude of 100 km. Besides that, Morpheus was not designed as a reusable rocket and is not able to carry humans to space. The design of the rocket should also allow for a quick assemble and disassemble of each section of the rocket to facilitate the study of each individual section in a modular rocket. Finally, it was also established from the beginning that the propellant and fuel would be LOx and LNG, respectively. From the literature review, it was evident that composite materials, especially CFRP composite laminates, are becoming an essential material in aerospace applications replacing metallic materials. Although composites allow for a reduction of weight when compared to metals, they also have some drawbacks. One main disadvantage is the incompatibility with liquid oxygen but also the additional difficulty in manufacture which increases the cost of the rocket. Nevertheless, in the conceptual design, the CFRP composite laminates was used in most of the components, except for the tanks, y-ring and downcomer. The y-ring should be welded to the tanks through the friction stir welding which provides a strong connection without additional weight. On the other hand, there are great concerns regarding the oxidation of aluminium parts when in contact with CFRP, especially if the aluminium component is much smaller. For this reason, the bolts used should be made out of titanium to solve this problem, even though this is a heavier material.

For the second part of this dissertation, the focus was on the thrust frame and aft skirt. Since this was a first iteration of this project, only an initial design was considered without any reinforcement in the

critical areas such as the holes. Besides that, it was not considered thermal protections. The simulations were carried out on the *NX Siemens* software. Three different materials were studied in these components of Morpheus, CFRP composites, aluminium alloy 2219-T851 and a sandwich composite with an aluminium honeycomb as the core and CFRP as the skin. The best design possible for the thrust frame that could resist the applied forces with a factor of safety of 1.44 and guaranteeing a reliable option consisted of a core with 24 mm and seven CFRP plies with 0.25 mm on each side. This amount to a total weight of 6.21 kg. On the other hand, for the aft skirt, a similar approach in the static analysis was done but an additional buckling analysis was simulated. Due to the complexity and dimensions of the aft skirt fuselage, different sections were considered. In the final design, the region below the thrust frame consisted of only three CFRP plies, while the rest of the aft skirt was made out of 2.25 mm in CFRP, with an additional 1 mm of aluminium at the top representing the Y-ring. This model has a mass of 6.83 kg. A door was also considered in this section to allow for a quick access to the interior of the rocket. The door could resist all the stresses with just 2 mm of CFRP plies making a total mass of 0.55 kg.

These final results were in line with what was expected since the composites represent a solution that has great mechanical properties with low density materials. Even though many simplifications were done, a factor of safety was considered which should result in the final design pointing towards the best direction.

6.2 Future Work

Since this was only the first iteration there are still many developments to be done in future work. The general design of the full rocket could still be changed due to a wide range of reasons such as cost, manufacture, or even changes in some requirements. However, even if none of the assumptions is changed, a detailed studied is still necessary. The areas of the holes will need a reinforcement and a thermal analysis must also be done. Moreover, the bonding between different face sheets and between the skin and the core must be studied in the future. Besides that, a special focus should be considered for the epoxy which could solve some of the problems of the compatibility problems while providing a strong bond between layers. Another aspect that should be studied is the welded connections, essential between the tanks and the y-ring.

Finally, all the work done during the development of this dissertation was based on the literature review of other models and simulations done by the *NX Siemens* software. However, when a clear image of the Morpheus is complete and after more components are studied, an experimental analysis should be performed.

Bibliography

[1] R. Lab. Rocket lab investor presentation, 2021. URL https://www.rocketlabusa.com/assets/Rocket-Lab-Investor-Presentation.pdf. Accessed on 10-08-2021.

[2] M. Sheetz. Bank of america expects the space industry to triple to a $1.4 trillion market within a decade. *CNBC*, October 2020.

[3] E. M. Marconi. What is a sounding rocket?, 2004. URL https://www.nasa.gov/missions/research/f_sounding.html. Accessed on 02-05-2021.

[4] G. Seibert. The history of sounding rockets and their contribution to european space research. *ESA Publications Division*, November 2006.

[5] G. A. C. Sr. The descriptive geometry of nose cones, 1996.

[6] S. M. Chowdhury. Design and performance simulation of a hybrid sounding rocket. Master's thesis, College of Agriculture, Engineering and Science, University of KwaZulu-Natal, December 2012.

[7] J. R. Spreiter. On the range of applicability of the transonic area rule. Technical Note 3673, NACA, Ames Aeronautical Laboratory Moffett Field, Calif., May . 1956.

[8] T. Owens. Polymer matrix composite material oxygen compatibility. In *Proceedings of the 4th Conference on Aerospace Materials, Processes, and Environmental Technology*, NASA Marshall Space Flight Center Huntsville, AL United States, February 2001. NASA.

[9] *Falcon user's guide*. Space Exploration Technologies Corp. (SpaceX), August 2020.

[10] S. L. H S Bang, Atanu Das. Friction stir lap joining of automotive aluminium alloy and carbon-fiber-reinforced plastic. In *IOP Conf. Ser.: Mater. Sci. Eng.*, 2018.

[11] E. C. for Space Standardization ECSS. Space engineering – mechanical – part 2: Structural. Technical Report ECSS-E-30 Part 2A, ESA - European Space Agency, April 2000.

[12] C. Staff. An introduction to the galvanic series: Galvanic compatibility and corrosion, 2020. URL https://www.corrosionpedia.com/an-introduction-to-the-galvanic-series-galvanic-compatibility-and-corrosion/2/1403. Accessed on 19-10-2021.

[13] K. Kowalczyk-Gajewska. *Micromeachanical Modelling of metals and alloys of high specific strength*. Instytut Podstawowych Problemów Techniki Polskiej Akademii nauk, 2011.

[14] Propellant combustion charts. URL `http://www.braeunig.us/space/comb-OM.htm`. Accessed on 21-10-2021.

[15] N. S. R.P. Reed, P.T. Purtscher. *Aluminum alloys for Als cryogenic tanks: comparative measurements of cryogenic mechanical properties of Al-Li alloys and Alloy 2219*. Phillips laboratory - Propulsion Directorate - Air Force systems command, Edwards Air Force base CA 93523-5000, February 1993.

[16] H. Y. Jinxin Meng, Yong Wang. Mechanical properties and internal microdefects evolution of carbon fiber reinforced polymer composites: Cryogenic temperature and thermocycling effects. *Elsevier*, (108083), February 2020.

[17] G. C. Zhan L.H. Analysis of research status of composite cryotank for space. *Aeronautical Manufact Technol*, 62(16):79–87, 2019.

[18] K. O. Yonemoto koichi, Yamamoto Yuta. Application of cfrp with high hydrogen gas barrier characteristics to fuel tanks of space transportation system. *Trans Japan Soc Aeronautical Space Space Technol Japan*, 7(26):8–13, 2019.

[19] F. L. Ni Liu, Bin Ma. Progress in research on composite cryogenic propellant tank for large aerospace vehicles. *Elvesier - Composites Part A*, 143(106297), 2021.

[20] Hexweb® aluminum flex-core® formable aluminum honeycomb, 2017. URL `https://www.hexcel.com/user_area/content_media/raw/HexWeb_AluminumFlexCore_DataSheet.pdf`. Accessed on 07-09-2021.

[21] Q. H. Jie Xu, Weixin Wang. Mechanical properties of pultruded high-temperature-resistant carbon-fiber-reinforced polymer tendons at elevated temperatures. *Elsevier - Construction and Building Materials*, 258(119526), 2020.

[22] W. Becker. *Archive of Applied Mechanics*, volume 68, chapter The in-plane stiffnesses of a honeycomb core including the thickness effect, pages 334–341. pringer-Verlag 1998, 1998.

[23] MatWeb. Aluminum 2219-t851. URL `http://www.matweb.com/search/datasheet_print.aspx?matguid=7ab8f01622894d1d93797dc899f621fa`. Accessed on 19-09-2021.

[24] S. Batchu. Rbe2 vs rbe3. URL `https://www.stressebook.com/rbe2-vs-rbe3/`. Accessed on 19-09-2021.

[25] P. P. Jonas Grünewald and V. Altstädt. Manufacturing of thermoplastic composite sandwich structures: A review of literature. *Journal of Thermoplastic Composite Materials*, 30(4):437–464, 2017.

[26] P. R. A. Muc, A. Stawiarski. Experimental investigations of compressed sandwich composite/honeycomb cylindrical shells. *Applied Composite Materials, An International Journal for the Science and Application of Composite Materials*, 25:177 – 189, June 2017.

Appendix A

Sounding Rocket Annexes

A.1 Rocket design

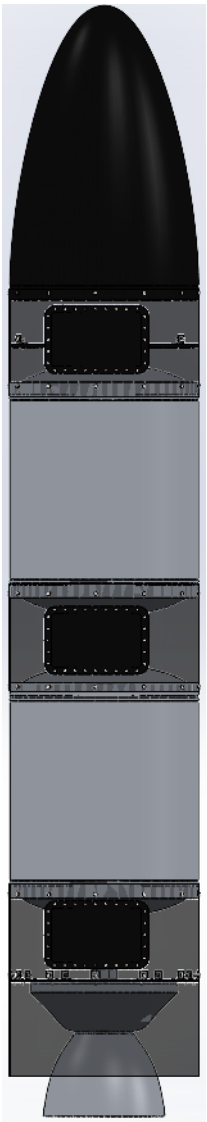

Figure A.1: Final design of the sounding rocket

(a) (b)

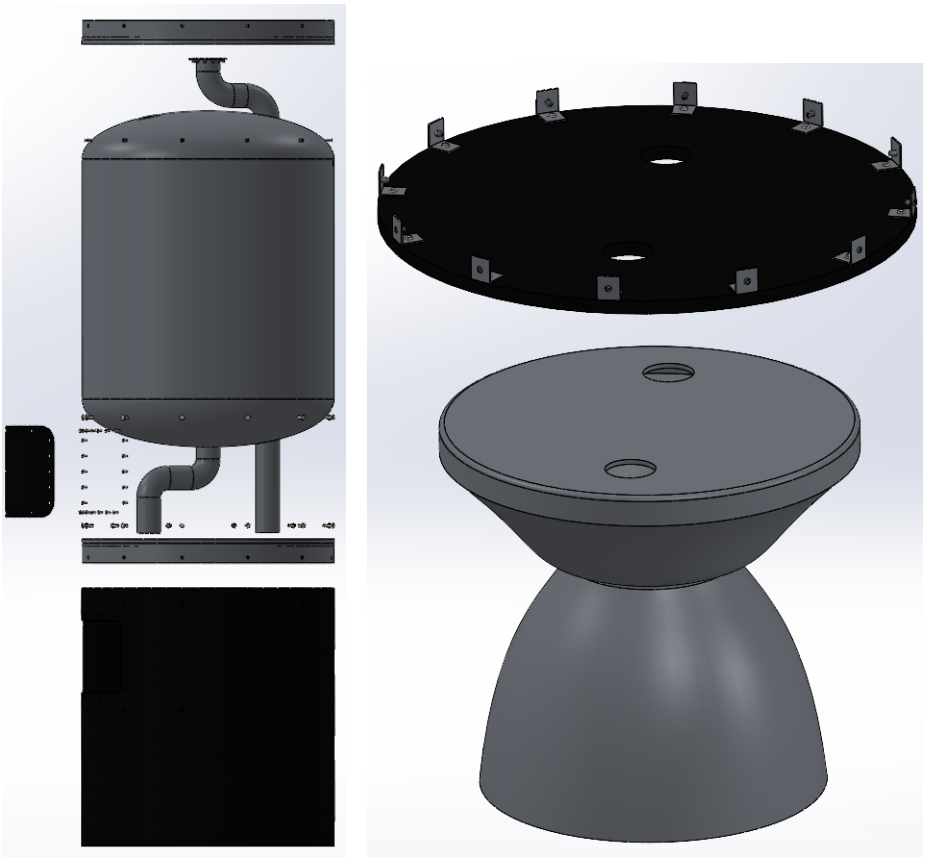

(c) (d)

Figure A.2: Exploded view of (a) nose cone and avionics (b) LOx tank (c) Fuel Tank (d) Motor

Atmospheric pressure				
Altitude	**Pressure [Pa]**			
10 550 m	27 000			
Sea level	100 000			
Pressure on base (Source: International Standard Atmosphere (ISA) data)				
Pressure on base, AoA 0 degrees				
Pressure on base, AoA 2 degrees				
Pressure on base, AoA 3 degrees				
Pressure on base, AoA 4 degrees				
Atmospheric pressure (0.1 MPa)				
External pressure (Source: International Standard Atmosphere (ISA) data)				
Pressure on base, AoA 0 degrees				
Pressure on base, AoA 2 degrees				
Pressure on base, AoA 3 degrees				
Pressure on base, AoA 4 degrees				
Atmospheric pressure (0.1 MPa)				
Pressure of main tanks				
Nominal pressure (0.5 MPa)				
Atmospheric pressure (0.1 MPa)				
	LOx tank		**LNG tank**	
Description	**Mass [kg]**	**Z coordinate [m]**	**Mass [kg]**	**Z coordinate [m]**
Half-full tanks	522,96	-2,76	177,95	-4,547
Full tanks	1058,76	-2,464	354,06	-4,294
Empty tanks (gas only)	9	-2,412	9	-4,136
Fixes mass				
Mass [kg]	**Z coordinate [m]**	**Location**		
34,198	-1,55	Forward skirt's plate		
12,118	-3,32	Aft skirt's plate		
233,405	-5,251	Thrust frame		
Variable mas				
Mass [kg]	**Z coordinate [m]**	**Location**	**Description**	
4,75	-1,55	Forward skirt's plate	Half-full	
4,75	-3,32	Intertank's plate	Half-full	
6,89	-5,251	Thrust frame	Full	
9,5	-1,55	Forward skirt's plate	Full	
9,5	-3,32	Intertank's plate		
6,89	-5,251	Thrust frame		
1	-1,55	Forward skirt's plate	Empty	
1	-3,32	Intertank's plate		
1	-5,251	Thrust frame		
Thrust				
Force [N]	**TVC [deg]**			
25250	0			
25250	8			
25000	0			
25000	2			
25000	4			
25000	6			
25000	8			
36300 (TBC)	0			
Linear acceleration				
X direction	**Y direction**	**Z direction**		
0 G	0 G	-1 G		
1.5 G	0.5 G	0.5 G		
Temperature				
LOx tank' temperature [K]	**LNG tank' temperature [K]**	**Other components' temperature [K]**		
90	110	300		

Figure A.3: Conditions for the Morpheus rocket

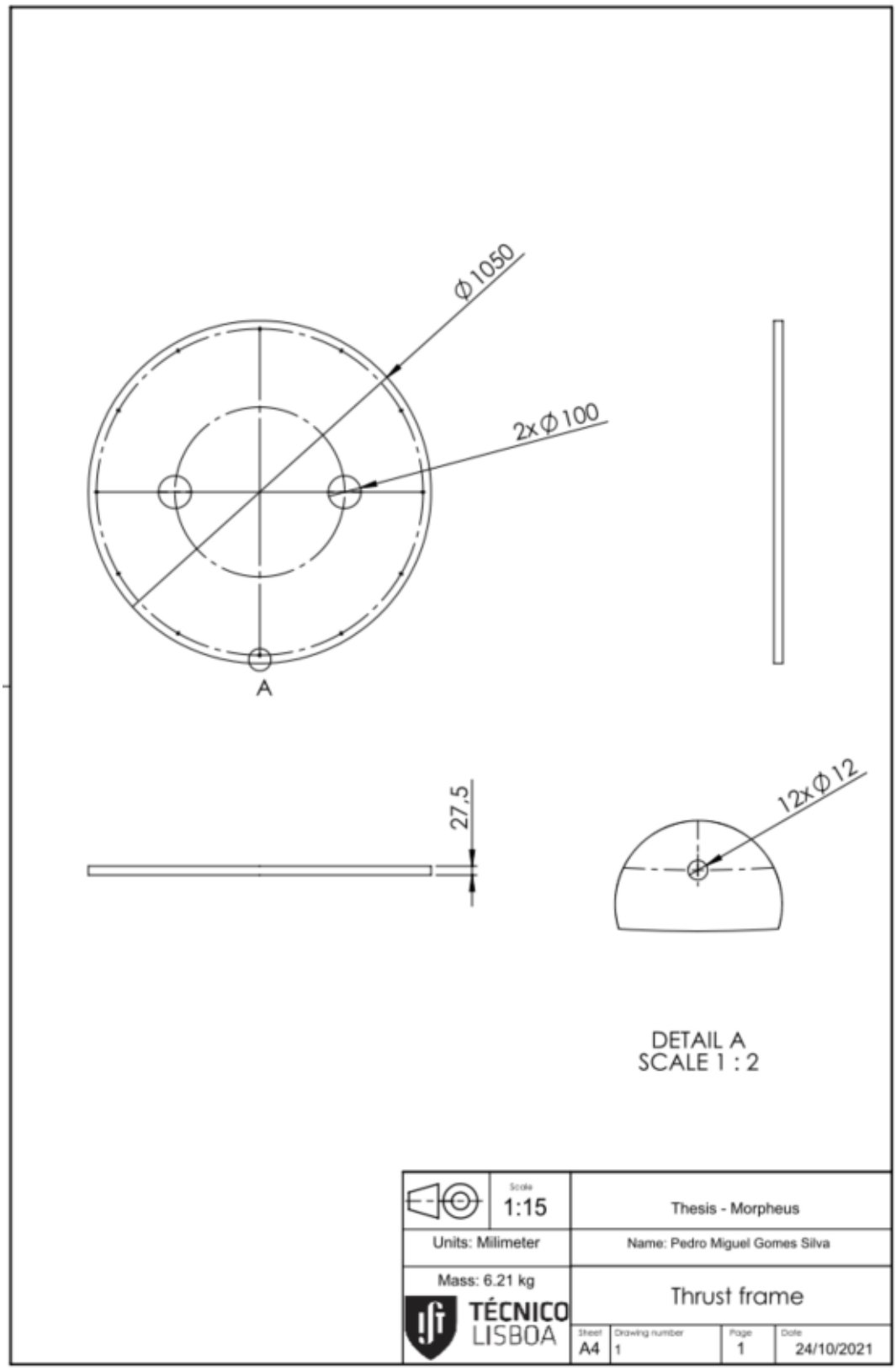

Figure A.4: Dimensions thrust frame

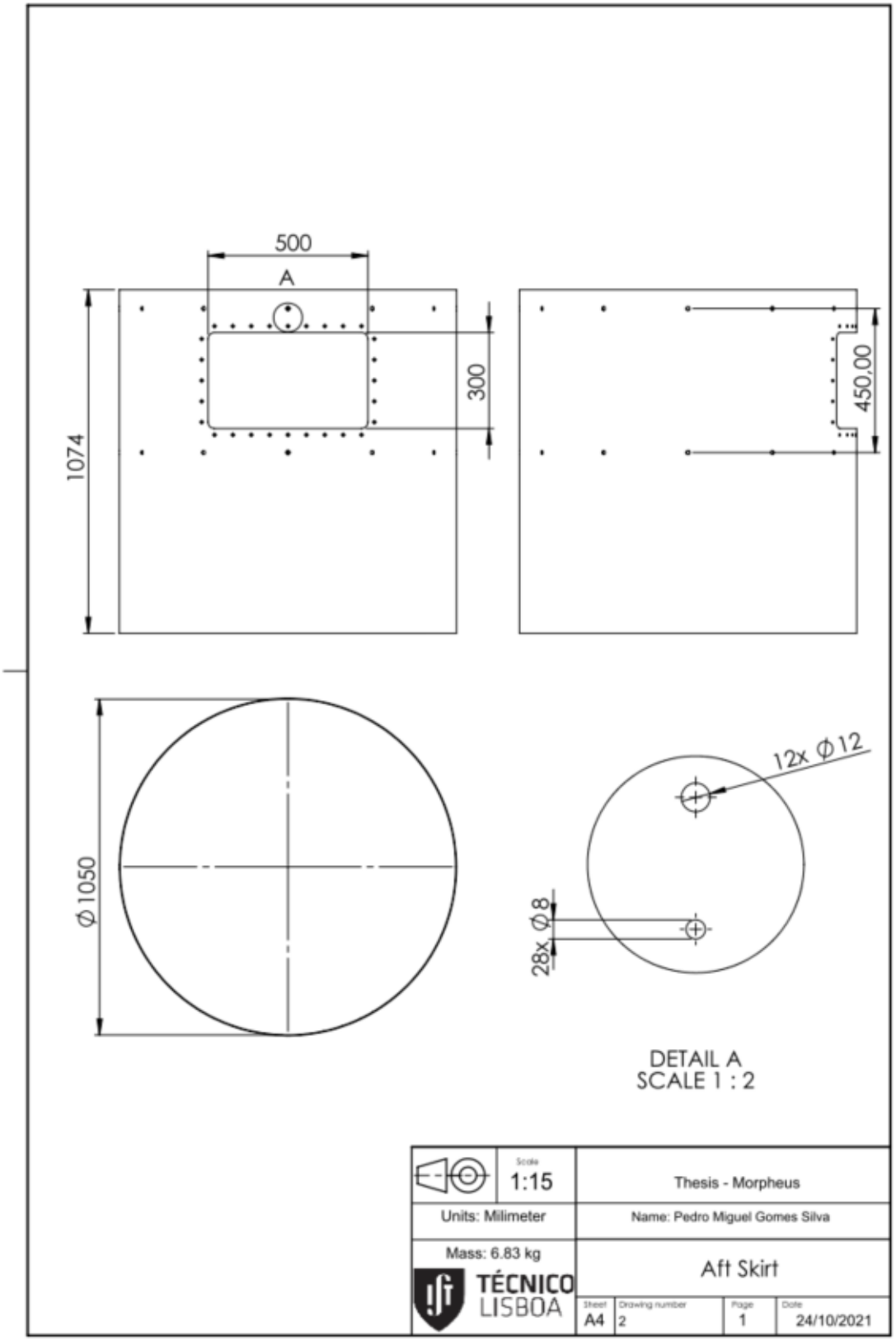

Figure A.5: Dimensions aft Skirt

A.2 Detailed results - static analysis

	Element Id	Node Id	Ply Id	Computation Location	Failure Theory Ply	Stresses						Failure Index Ply
						Stress11 mN/mm^2(kPa)	Stress22 mN/mm^2(kPa)	Stress33 mN/mm^2(kPa)	Stress12 mN/mm^2(kPa)	Stress23 mN/mm^2(kPa)	Stress31 mN/mm^2(kPa)	Unitless
Max Absolute Stress 11	21059	21681	2	Bottom	Tsai-Wu	**1,75E+05**	-2,15E+04	0,00E+00	1,14E+04	9,62E+00	7,89E+01	5,44E-01
Max Absolute Stress 22	21056	21678	1	Bottom	Tsai-Wu	-3,34E+04	**2,37E+05**	0,00E+00	-6,39E+00	0,00E+00	0,00E+00	9,69E-01
Max Absolute Stress 33	9136	8757	1	Bottom	Tsai-Wu	1,26E+05	1,10E+05	**0,00E+00**	1,27E+03	0,00E+00	0,00E+00	4,99E-01
Max Absolute Stress 12	21056	21678	2	Bottom	Tsai-Wu	9,45E+04	9,87E+04	0,00E+00	**2,25E+04**	-1,09E+01	1,00E+01	7,00E-01
Max Absolute Stress 23	30866	30991	6	Top	Tsai-Wu	1,32E+04	-1,45E+04	0,00E+00	2,81E+03	**-2,29E+03**	6,56E+02	7,58E-03
Max Absolute Stress 31	30865	30989	8	Middle	Core Shear	1,34E-05	2,20E-05	0,00E+00	3,58E-05	-8,02E+02	**2,78E+03**	7,78E-01
Max Absolute Ply Failure Index	21056	21678	1	Bottom	Tsai-Wu	-3,34E+04	2,37E+05	0,00E+00	-6,39E+00	0,00E+00	0,00E+00	**9,69E-01**

Figure A.6: Maximum stress and failure index for the final thrust frame with 24 mm of an aluminium honeycomb's core and 7 plies of 0.25 mm carbon fiber on each side

	Element Id	Node Id	Ply Id	Global Ply Id	Computation Location	Laminate Name	Failure Theory Ply	Stresses						Failure Index Ply
								Stress11 mN/mm^2(kPa)	Stress22 mN/mm^2(kPa)	Stress33 mN/mm^2(kPa)	Stress12 mN/mm^2(kPa)	Stress23 mN/mm^2(kPa)	Stress31 mN/mm^2(kPa)	Unitless
Max Absolute Stress 11	184991	182158	9	202	Top	Laminate1	Tsai-Wu	**-2,43E+05**	-7,31E+04	0,00E+00	4,52E+03	-5,79E-12	-1,20E-11	7,14E-01
Max Absolute Stress 22	184992	182157	8	179	Top	Laminate1	Tsai-Wu	-4,15E+04	**-2,05E+05**	0,00E+00	1,09E+04	4,51E+03	-1,07E+03	5,93E-01
Max Absolute Stress 33	162381	162761	1	184	Bottom	Laminate2	Tsai-Wu	-3,56E+03	4,60E+03	**0,00E+00**	8,85E+02	0,00E+00	0,00E+00	2,25E-03
Max Absolute Stress 12	185332	179274	1	1	Bottom	Laminate1	Tsai-Wu	2,18E+04	6,62E+04	0,00E+00	**6,95E+04**	0,00E+00	0,00E+00	N/A
Max Absolute Stress 23	184992	182157	4	175	Top	Laminate1	Tsai-Wu	2,03E+04	-5,17E+04	0,00E+00	5,51E+03	**1,33E+04**	-3,21E+03	4,38E-02
Max Absolute Stress 31	184991	182158	4	175	Top	Laminate1	Tsai-Wu	9,83E+03	-3,40E+04	0,00E+00	5,86E+03	4,91E+03	**-1,38E+04**	2,60E-02
Max Absolute Ply Failure Index	184992	182157	9	202	Top	Laminate1	Tsai-Wu	-2,14E+05	-7,82E+04	0,00E+00	1,56E+04	-3,55E-12	3,88E-12	**7,15E-01**

Figure A.7: Maximum stress and failure index for the final aft skirt with an 1 mm aluminium Y-ring, a lower fuselage with 0.75 mm of carbon fiber and the rest of the fuselage with 2.25 mm of CFRP. The door has 0.75 mm of CFRP